AD NUMBER
ADB011346
LIMITATION CHANGES

TO:

Approved for public release; distribution is unlimited.

FROM:

Distribution authorized to U.S. Gov't. agencies only; Test and Evaluation; MAY 1976. Other requests shall be referred to Air Force Aero-Propulsion Lab., Wright-Patterson AFB, OH 45433.

AUTHORITY
AFAWL ltr 16 Sep 1976

AEDC-TR-76-76

PERFORMANCE AND OPERATING CHARACTERISTICS
OF A TURBINE ENGINE PROPULSION SIMULATOR
AT SIMULATED FLIGHT CONDITIONS

ENGINE TEST FACILITY
ARNOLD ENGINEERING DEVELOPMENT CENTER
AIR FORCE SYSTEMS COMMAND
ARNOLD AIR FORCE STATION, TENNESSEE 37389

May 1976

Final Report for Period April 8 — June 18, 1975

Prepared for

AIR FORCE AERO-PROPULSION LABORATORY (TBP)
WRIGHT-PATTERSON AIR FORCE BASE, OHIO 45433

NOTICES

APPROVAL STATEMENT

This technical report has been reviewed and is approved for publication.

FOR THE COMMANDER

CHAUNCEY D. SMITH, JR.
Lt Colonel, USAF
Chief Air Force Test Director, ETF
Directorate of Test

CRAIG E. MAHAFFY
Colonel, USAF
Director of Test

UNCLASSIFIED

REPORT DOCUMENTATION PAGE		READ INSTRUCTIONS BEFORE COMPLETING FORM
1 REPORT NUMBER AEDC-TR-76-76	2 GOVT ACCESSION NO.	3 RECIPIENT'S CATALOG NUMBER
4 TITLE (and Subtitle) PERFORMANCE AND OPERATING CHARACTERISTICS OF A TURBINE ENGINE PROPULSION SIMULATOR AT SIMULATED FLIGHT CONDITIONS		5 TYPE OF REPORT & PERIOD COVERED Final Report – April 8 – June 18, 1975
		6 PERFORMING ORG REPORT NUMBER
7 AUTHOR(s) J. O. Brooks and R. A. Wasson, Jr. ARO, Inc.		8 CONTRACT OR GRANT NUMBER(s)
9 PERFORMING ORGANIZATION NAME AND ADDRESS Arnold Engineering Development Center (XO) Air Force Systems Command Arnold Air Force Station, Tennessee 37389		10 PROGRAM ELEMENT, PROJECT, TASK AREA & WORK UNIT NUMBERS Program Element 63202F, Project 668A, Task 02
11 CONTROLLING OFFICE NAME AND ADDRESS Air Force Aero-Propulsion Laboratory (TBP) Wright-Patterson Air Force Base, Ohio 45433		12 REPORT DATE May 1976
		13 NUMBER OF PAGES 80
14 MONITORING AGENCY NAME & ADDRESS(if different from Controlling Office)		15 SECURITY CLASS. (of this report) UNCLASSIFIED
		15a DECLASSIFICATION/DOWNGRADING SCHEDULE N/A

16 DISTRIBUTION STATEMENT (of this Report)

Distribution limited to U. S. Government agencies only; this report contains information on test and evaluation of military hardware; May 1976; other requests for this document must be referred to Air Force Aero-Propulsion Laboratory, Wright-Patterson Air Force Base, Ohio 45433.

17 DISTRIBUTION STATEMENT (of the abstract entered in Block 20, if different from Report)

18 SUPPLEMENTARY NOTES

Available in DDC

19 KEY WORDS (Continue on reverse side if necessary and identify by block number)

simulator	distortion
scale model	Reynolds number
turbofan engine	transonic flow
performance stability	altitude simulation

20 ABSTRACT (Continue on reverse side if necessary and identify by block number)

An investigation was conducted on an engine propulsion simulator (S/N 002/2) to determine the compressor operating maps at compressor inlet pressures of 7, 12, and 16 psia at an inlet total temperature of 120°F with both dry and reheat mixer/nozzle configurations, to determine the dry and reheat nozzle entrance pressure and temperature distortion with the anti-distortion screens installed upstream of the nozzle, and to determine nozzle thrust and

DD $_{1 \, JAN \, 73}^{FORM}$ 1473   EDITION OF 1 NOV 65 IS OBSOLETE

UNCLASSIFIED

20. ABSTRACT (Continued)

nozzle flow coefficients at simulated altitude/Mach number flight
conditions of 12,700/0.6, 21,400/0.8, 24,800/0.9, 34,200/1.2, and
43,700/1.5 with both mixer/nozzle configurations. Compressor maps
and nozzle performance are presented and compared with the pre-
dicted values. Nozzle entrance pressure and temperature distor-
tions are presented. In addition, simulator operational experi-
ences are discussed.

AFSC
Arnold AFS Tenn

PREFACE

The work reported herein was conducted by the Arnold Engineering Development Center (AEDC), Air Force Systems Command (AFSC), at the request of the Aero-Propulsion Laboratory (AFAPL), AFSC, Wright-Patterson, AFB, Ohio, under Program Element 63202F/668A-02. The propulsion simulator was furnished by the General Electric Company, Cincinnati, Ohio. The results were obtained by ARO, Inc. (a subsidiary of Sverdrup & Parcel and Associates, Inc.), contract operator of AEDC, AFSC, Arnold Air Force Station, Tennessee. The test was conducted in the Propulsion Research Area (R-2C-4) of the Engine Test Facility (ETF) under ARO Project No. R41E-02A. The authors of this report were J. O. Brooks and R. A. Wasson, Jr., ARO, Inc. Data reduction was completed on December 1, 1975, and the manuscript (ARO Control No. ARO-ETF-TR-76-21) was submitted for publication on March 2, 1976.

CONTENTS

ILLUSTRATIONS

TABLE

1.0 INTRODUCTION

The multimission engine propulsion simulator is a 0.085-scale version of a mixed-flow, augmented turbofan engine. The simulator is designed to simultaneously simulate corrected compressor inlet airflow, nozzle pressure ratio, and nozzle flow function.

The primary purpose of the engine propulsion simulator is to provide simultaneous simulation of inlet and exhaust flow fields in a full-span, multimission, aircraft model, thereby allowing direct determination of aircraft/propulsion system performance at angle of attack and/or yaw for a wide range of flight conditions. When combined with an aircraft scale model in a wind tunnel test, the engine propulsion simulator can also be used as a tool for identification of system performance improvements before and during flight operations (Ref. 1). Previous testing conducted at AEDC on the propulsion simulator is reported in Refs. 2 and 3.

A test program was conducted in compliance with the General Electric furnished test plan (Ref. 4). The test objectives were to (1) perform compressor mapping at compressor inlet pressures of 7, 12, and 16 psia at an inlet temperature of 120°F with both dry and reheat mixer/nozzle configurations, (2) determine the dry and reheat nozzle entrance pressure and temperature distortion, (3) and determine nozzle airflow and thrust characteristics at simulated altitude/Mach numbers of 12,700/0.6, 21,400/0.8, 24,800/0.9, 34,200/1.2, and 43,700/1.5 with both mixer/nozzle configurations.

The results of the test program are presented herein. Compressor operating maps, nozzle entrance pressure and temperature distortion, and the nozzle airflow and thrust characteristics are presented and discussed for both the dry (nonaugmented) and reheat (augmented) mixer/nozzle configurations. In addition, operational experiences and difficulties encountered during the program are discussed.

2.0 APPARATUS

2.1 TEST ARTICLE

The multimission engine propulsion simulator (Fig. 1) is a 0.085-scale version of a mixed-flow, augmented turbofan engine. The simulator inlet is 3.0 in. in diameter, and total simulator length (with nozzle extension and reheat nozzle) is 29 in. The nominal weight of the simulator assembly is 38 lb.

2.1.1 Compressor

The four-stage, single-rotor axial compressor has an overall design pressure ratio of 2.82 and a sea-level-static design airflow of 1.554 lbm/sec at a (100-percent-rated) rotor speed of 75,185 rpm. The compressor airflow is ducted directly from the compressor discharge station to the exhaust nozzle, thereby bypassing the turbine (Fig. 1c).

2.1.2 Turbine

The single-stage turbine is driven by an external high-pressure air source. The single compressor/turbine rotor is supported by forward and aft bidirectional bearings which are lubricated by an external oil flow system (Fig. 2). To aid bearing seating and improve rotor stability, a preset aft load of 55 lbf is applied to the rotor during installation (Ref. 4). To maintain this negative loading during all operating conditions, the cavity aft of the turbine is partially vented by the rotor thrust trim orifice in the mixer.

The high-pressure turbine drive air enters an annular manifold at a forward plane of the simulator through a 0.66-in.-diam port perpendicular to the simulator centerline (Figs. 1b and c). From the manifold, the air flows axially aft along the periphery of the simulator through five, 0.25-in.-diam channels, then enters five sets of two radial holes (0.25- and 0.16-in.-diam) in each of five struts leading to the turbine drive air plenum just upstream of the turbine nozzles (Fig. 1c). After passing axially through the turbine, the air turns outward 90 deg through two elliptical passages (0.28 by 0.125 in. wide) in the five struts to an annular manifold and then flows axially forward through five pairs of similar channels around the simulator periphery to centerline through a 1.66-in.-diam port (Figs. 1b and c). A small amount (nominally 1 percent) of the turbine discharge airflow is bled into the mixer (Fig. 1c) to provide a rotor thrust balance pressure. The bleed air is discharged axially through an orifice on the mixer centerline into the compressor discharge airflow in the nozzle.

2.1.3 Mixers and Nozzles

A mixer assembly, located downstream of the turbine (Fig. 1c), is designed to permit turbine drive air to bleed and mix with the compressor airflow to obtain a desired simulation of full-scale nozzle pressure ratio and nozzle flow function. The mixer designs utilize radial and/or axial injection of air through choked orifices from a conical afterbody. Three mixer configurations—a solid mixer (G.E. P/N 341), a dry mixer (G.E. P/N C-15948) (Fig. 1d), and a reheat mixer (G.E. P/N C-16893)(Fig. 1e)—were used during the program. All configurations incorporated a single axial rotor thrust trim orifice (0.185-in. ID).

Two nozzle configurations were used during the program: a dry nozzle (G.E. P/N D-16825)(Fig. 1f) with a throat area of 3.120 in.^{2} and a reheat nozzle (G.E. P/N D-16826)(Fig. 1g) with a throat area of 5.718 in.^{2}. The dry nozzle, with the solid mixer (motor mode), was used during initial testing. The dry and reheat nozzles, with the dry and reheat mixer, respectively, were used to determine the dry and reheat compressor maps, nozzle pressure and temperature distortion, and nozzle performance.

A nozzle extension section, approximately 3.75 in. in diameter (ID), was installed between the mixer and the nozzle to provide additional mixer airflow and compressor inlet airflow mixing length.

2.2 INSTALLATION

2.2.1 Engine Propulsion Simulator

The simulator and associated inlet assembly were secured to a thrust stand suspended from the top of the test chamber located in the Propulsion Research Test Area (R-2C-4). The engine propulsion simulator installation is shown in Fig. 3.

The simulator inlet assembly consists of a bellmouth with a 3:2 ratio elliptical inlet. The compressor inlet air system is shown schematically in Fig. 3a. The system was capable of supplying conditioned airflow up to 1.8 lbm/sec at the required compressor inlet pressure (up to 16 psia) and temperature. Supply air temperature control was provided by a steam-air heat exchanger which maintained the desired compressor inlet air temperature at 120 ± 5°F. A critical-flow airflow-measuring venturi was used to measure the compressor inlet airflow. An inlet air seal (Fig. 3b) between the bellmouth (which is mounted to the test chamber) and the simulator prevented flow leakage.

Air from the simulator exhaust nozzle was discharged from the test chamber through a 6-in.-diam exhaust duct.

2.2.2 Turbine Drive Air System

The facility high-pressure turbine drive air system is shown schematically in Fig. 4. The system was capable of supplying conditioned airflow up to 5.30 lbm/sec at the required turbine inlet pressure (up to 1,300 psia) and temperature. Supply air temperature control was provided by a steam-air heat exchanger which maintained the desired turbine inlet air temperature at 200 ± 3°F. Critical-flow airflow-measuring venturis were used to measure turbine drive and turbine drive bleed airflow. Emergency shutoff valves were included in the turbine drive air system (Fig. 4) to automatically shut off air to the turbine and

7

simultaneously vent air from the turbine inlet manifold in the event critical operational parameters exceeded prescribed levels (see Section 2.2.3).

2.2.3 Emergency Shutdown System

The emergency shutdown system was designed to rapidly unload the simulator by shutting off the turbine drive air and venting the turbine drive inlet manifold to ambient pressure (Fig. 4). The emergency shutdown system is comprised of two 1-in. solenoid valves which are automatically operated upon reaching preset values of (1) bearing temperature level or rate of rise, (2) rotor speed level or rate of rise, (3) turbine inlet temperature and/or pressure level, or (4) vibration "g" level. The bearing temperature controllers were equipped with contacts which close and activate the solenoid valve when a preset bearing temperature level is exceeded. The speed shutdown system converts a frequency signal from the General Electric-supplied speed pickup to an analog signal which is used to activate the emergency shutoff valve solenoids. The turbine inlet shutdown system is activated by contacts which close when a preset turbine inlet pressure or temperature level is exceeded. The acceleration shutdown system is activated by a contact contained within the accelerometer amplifier which closes when a preset "g" level is exceeded.

When the emergency shutdown system is activated, the following valve operating sequence occurs:

1.   The turbine drive air emergency shutoff valve is closed,

2.   The turbine drive air emergency dump valve is opened, and

3.   The turbine drive bypass valve is opened.

The turbine drive air safety valves operated full travel (open to closed or closed to open) in 60 to 65 msec from application of the shutoff signal to the valve solenoid. Turbine inlet pressure decayed to ambient conditions in approximately 0.5 sec when the valves were activated at rated compressor rotor speed of 75,185 rpm and at a turbine inlet pressure of 760 psia (Ref. 3).

2.2.4 Simulator Control Console

A simulator control console, supplied by General Electric and described in detail in Ref. 5, was used during this test program to control and monitor the critical operating parameters of the simulator. The control console, shown in Fig. 5, was designed as a rotor speed control device to remotely control two engine propulsion simulators

simultaneously or independently in a wind tunnel or other test facility. The console panel is divided into two sections for operation of two simulators. Each panel contains controls and annunciators common to the system operation. The console controls a separate hydraulic supply system which positions the turbine drive air inlet and bleed control valves and thereby sets simulator rotor speed (rpm). The console has a feedback design such that a selected simulator rotor speed is maintained. Provisions are incorporated into the console to operate the simulator in one of three modes: a manual mode, which does not have a speed (rpm) feedback control; an analog mode, which permits continuous variations of speed; and a digital mode, which has a feedback speed control, thus maintaining a selected speed. Provisions are also incorporated for acceleration and deceleration of the simulator from one speed level to another desired speed at a rate of up to 10,000 rpm/sec. The console also monitors the critical operating parameters of the simulator and provides automatic simulator shutdown protection in case preset limits of rotor overspeed, bearing temperatures, bearing temperature rate of rise, vibration "g" level, turbine drive air inlet pressure, or turbine drive air inlet temperature are exceeded or there is a loss in hydraulic pressure to the control valves.

2.2.5 Lube Oil

A continuous flow of MIL-L-23699 lube oil was supplied to the simulator front and rear bearings by a two-channel mini-pump oil system (Fig. 2a). Flow rates to the front and rear bearings main oil systems were· nominally 23 and 20 cc/hr, respectively. The oil scavange system (Fig. 2a) supplied an electronic signal which monitored the oil scavange to ensure lubrication of the bearings.

2.3 INSTRUMENTATION

Instrumentation was provided to measure engine propulsion simulator aerodynamic pressures and temperatures, rotor speed, thrust, and other simulator and test cell system parameters as required for proper and safe operation of the engine simulator. Pressure and temperature sensors for the simulator were located at the stations shown in Fig. 6a. Diagrams showing the number and type of instrumentation installed at each station are shown in Fig. 6b.

Steady-state aerodynamic pressures were measured with strain-gage-type transducers, and temperatures were measured with Chromel®-Alumel® (CA), Iron-Constantan (IC), or Copper-Constantan (CC) thermocouples. The millivolt outputs of the transducers were recorded on magnetic tape using a high-speed analog-to-digital data acquisition system and converted to engineering units and calculated performance parameters by a high-speed digital computer. Selected channels of pressure, temperature, acceleration, and vibration were displayed in the control room for monitoring and manual recording.

Engine rotor speed was measured with a variable-reluctance magnetic pickup whose output signals were converted from a frequency-to-analog signal and then recorded on an analog-to-digital data acquisition system. Speed was also displayed in the control room on variable-time-base electronic counters.

Magnetic tape in the frequency modulation mode was used to record transient engine simulator performance. Transient aerodynamic pressures were measured throughout the engine with close-coupled strain-gage-type transducers.

High-response static pressure instrumentation consisted of four piezoelectric pressure transducers, two each located at the compressor inlet (station 2) and discharge (station 13) to detect high-frequency pressure fluctuations occurring during compressor surge conditions. These data were recorded in the frequency modulation mode on magnetic tape and visually displayed on oscilloscopes in the control room.

The instrumentation ranges, measurement and recording methods, and an estimate of the steady-state measurement uncertainties are presented in Table 1.

2.4 CALIBRATION

All transducer and system calibrations performed during this test are traceable to the National Bureau of Standards (NBS). Each link in the traceability chain to the NBS is maintained and documented by the AEDC Standards Laboratory (Ref. 6).

The aerodynamic pressure measurement transducers utilized in the Automatic Multiple Pressure Scanning (AMPS) System (Table 1), as well as other pressure transducers, were pretest calibrated in the Standards Laboratory. Before and after each test period, these transducer systems were calibrated by an electrical, four-step calibration, using precision resistors in the transducer circuits to simulate selected pressure levels.

Calibration data for the piezoelectric pressure transducers were provided by the manufacturer.

Lubrication oil flow level was measured by a capacitance-type liquid level gage, and the lube oil flow rate was calculated.

The temperature transducers (thermocouples) were fabricated from wire conforming to Instrument Society of America Specifications. Before and after each test period, known millivolt levels were applied to each temperature recording system, and the corresponding temperature equivalents were obtained from 150°F reference tables based on the NBS temperature versus millivolt tables. Nonlinearity in the thermocouple characteristics was accounted for in the data reduction program.

The vibration transducers were calibrated in the Standards Laboratory to establish their displacement versus voltage output relationship. Before and after each test period, the vibration recording systems were calibrated by applying known voltage input levels measured with a calibrated voltmeter.

The thrust measuring system was in-place calibrated by applying to the thrust stand force levels which were measured with force transducers (load cells) calibrated in the Standards Laboratory. During the in-place calibration, resistance shunt equivalent forces for the data load cell were determined. Before and after each test period, multiple step resistance shunt calibrations were performed to calibrate each recording channel of the measuring system.

The rotor speed measuring system transducer (variable-reluctance magnetic pickup) characteristics of rotational speed versus frequency were supplied by the General Electric Co. Before and after each test period, the speed recording systems were calibrated by applying known frequency input levels from a calibrated frequency generator.

3.0 PROCEDURE

3.1 TEST CONDITIONS

Compressor mapping was conducted at compressor inlet pressures of 7, 12, and 16 psia. The compressor inlet total temperature was maintained constant (120 ± 5°F) over the entire compressor inlet airflow range (0.35 to 1.70 lbm/sec). The compressor inlet air system was designed and fabricated by AEDC personnel. The simulator exhausted to a test chamber pressure of 7, 12, and 14.2 psia for compressor inlet pressures of 7, 12, and 16 psia, respectively.

Nozzle performance testing was conducted at the following simulated flight conditions:

Mach Number	Altitude, ft
0.6	12,700
0.8	21,400
0.9	24,800
1.2	34,200
1.5	43,700

Simulated flight conditions were set as follows:

1. The test cell pressure (P_{AMB}) was reduced to set the required altitude.

2. The compressor inlet total temperature (T_2) was maintained constant (120 ± 5°F).

3. The compressor inlet pressure (P_2) was increased to set the required Mach number.

Turbine drive air was supplied to the turbine drive manifold at a pressure (up to 1,800 psia) required to set the desired rotor speed. The turbine drive air temperature was controlled to 200 ± 3°F.

3.2 SIMULATOR OPERATING LIMITS

The following simulator maximum operating limits, established by the General Electric Company (Ref. 3), were observed during all simulator operation:

Compressor Inlet Pressure	16 psia
Compressor Inlet Temperature	180°F
Compressor Discharge Pressure	55 psia
Compressor Discharge Temperature	500°F
Turbine Inlet Pressure	1,500 psia
Turbine Inlet Temperature	250°F
Turbine Exit Pressure	650 psia
Mixer Entrance Pressure	650 psia
Forward Bearing Temperature	250°F
Aft Bearing Temperature	225°F
Bearing Temperature Rate of Rise	3.0°F/sec (during steady-state operation)
Vibration	6 g's
Speed	86,000 rpm

3.3 TEST PROCEDURE

The desired rotor speed is set by partially opening the turbine drive inlet air control valve with the turbine drive air bleed valve in the full open position.

The procedure used to determine the dry and reheat compressor maps was to obtain steady-state data on the minimum operating line at various corrected compressor inlet airflow rates with the turbine drive air bleed valve in the full open position. The turbine drive air bleed valve was then partially closed to back pressure the mixer cavity, while maintaining a constant corrected rotor speed, to inbleed airflow through the choked mixer orifices into the nozzle to mix with the compressor airflow. Steady-state data were obtained at several points while increasing the mixer inbleed airflow rate, loading the compressor toward its surge line. This procedure was continued until any of the following occurred: (1) the turbine drive air bleed valve was in the full closed position, (2) the mixer entrance pressure limit was reached, or (3) incipient compressor surge was detected. Incipient compressor surge was determined by monitoring the compressor inlet (PS_2) and compressor exit (PS_{13}) high-response static pressure instrumentation for a rapid increase in pressure fluctuations as typically shown in Fig. 7. When incipient compressor surge was indicated, the compressor loading was decreased by opening the turbine drive air bleed valve. A steady-state data point was recorded near the incipient compressor surge line to obtain the maximum operating line.

Nozzle performance test conditions were set according to the desired altitude and Mach number. Then the turbine drive air inlet control was opened to set the desired corrected compressor inlet airflow, and the turbine drive air bleed valve was closed to set the desired compressor pressure ratio. When all conditions were stable, a steady-state data point was recorded.

3.4 CALCULATIONS

The methods used to calculate steady-state parameters are presented in Appendix A.

4.0 RESULTS AND DISCUSSION

An investigation was conducted on an engine propulsion simulator to (1) determine the compressor operating maps at compressor inlet total pressures of 7, 12, and 16 psia at an inlet total temperature of 120°F with both dry and reheat mixer/nozzle configurations, (2) determine the dry and reheat nozzle entrance total pressure and temperature distortion with the anti-distortion screens installed upstream of the nozzle, and (3) determine nozzle airflow and nozzle thrust flow coefficients at simulated altitude/Mach number flight conditions of 12,700/0.6, 21,400/0.8, 24,800/0.9, 34,200/1.2, and 43,700/1.5 with both mixer/nozzle configurations.

The simulator was operated at corrected rotor speeds ranging from approximately 34,000 to 83,000 rpm. Rated rotor speed at sea-level-static conditions was 75,185 rpm.

The compressor maps and the airflow and thrust characteristics with the dry and reheat nozzle configurations are presented and compared with predicted performance (Ref. 4). Also presented are the nozzle entrance total pressure and temperature distortions.

4.1 COMPRESSOR MAPPING

The minimum operating lines (P_{13}/P_2 versus $WA_2\sqrt{\theta_2}/\delta_2$) of the dry and reheat configuration were obtained by operating with the turbine drive bleed valve in the full open position, providing minimum turbine bleed airflow through the mixer orifices into the nozzle. The maximum operating line was obtained by closing the turbine drive bleed valve to increase airflow through the mixer orifices into the nozzle, loading the compressor, while maintaining constant corrected rotor speed. High-response compressor inlet (PS_2) and compressor exit (PS_{13}) static pressure instrumentation was used to indicate incipient compressor surge. Incipient compressor surge was indicated with the dry mixer/nozzle configuration. The maximum operating line for the reheat mixer/nozzle configuration was obtained by closing the bleed until any of the following occurred: (1) the bleed valve was in the full closed position, (2) the compressor pressure ratio was within 5 percent of the surge line value determined during compressor mapping in the dry configuration, or (3) the mixer entrance pressure limit (P_{57} = 650 psia) was reached.

4.1.1 Dry Configuration

The simulator compressor maps with the dry nozzle configuration are shown in Fig. 8 for compressor inlet pressures of 7, 12, and 16 psia at an inlet temperature of 120°F. For an inlet total pressure of 7 psia and a constant corrected airflow of 1.60 lbm/sec (predicted airflow at rated speed), the compressor pressure ratio increased from 2.68 (5.6 percent lower than predicted) on the minimum operating line (Fig. 8a) to 3.28 (as predicted) at the surge line, resulting in a stability margin of 22.4 percent.

The stability margin at a constant corrected compressor inlet airflow of 1.60 lbm/sec was 23.4 and 25.9 percent for compressor inlet pressures of 12 (Fig. 8b) and 16 (Fig. 8c) psia, respectively. This increase in stability margin as inlet pressure increased from 7 to 16 psia is attributed to the effect of Reynolds number index (Ref. 2).

4.1.2 Reheat Configuration

The simulator compressor maps with the reheat nozzle configuration are shown in Fig. 9 for compressor inlet pressures of 7, 12, and 16 psia at an inlet temperature of 120°F. For an inlet pressure of 7 psia and a constant corrected airflow of 1.60 lbm/sec, the compressor pressure ratio ranged from 2.09 (4.1 percent lower than predicted) to 3.28 (determined during compressor mapping with the dry nozzle configuration) at the surge line, resulting in a stability margin of 56.9 percent.

14

The stability margin at a constant corrected compressor inlet airflow of 1.60 lbm/sec was 58.1 percent for a compressor inlet pressure of 12 psia (Fig. 9b). This increase in stability margin as inlet pressure increased from 7 to 12 psia is attributed to the effect of Reynolds number index (Ref. 2).

Since the compressor surge line is not a function of mixer/nozzle configuration, the surge line determined in the dry configuration was not repeated in the reheat configuration. For corrected rotor speeds below 70 percent, the mixer airflow limit was reached (turbine bleed valve full closed) prior to obtaining the surge pressure ratio. This operating limit is presented and compared to that predicted in Fig. 9. At an inlet pressure of 16 psia (Fig. 9c) for corrected rotor speeds above approximately 85 percent, the mixer entrance pressure limit (650 psia) was reached prior to obtaining the surge pressure ratio. This operating limit is presented and compared to that predicted in Fig. 9c.

4.2 NOZZLE PRESSURE AND TEMPERATURE DISTORTION

The dry and reheat nozzle entrance pressure and temperature distortion, ((MAX - MIN)/AVG), as a function of corrected compressor airflow are presented in Fig. 10. The dry nozzle entrance pressure distortion was less than 2.0 percent for all values of corrected compressor airflow (Fig. 10a). For a constant corrected compressor airflow of 1.60 lbm/sec, the dry nozzle entrance temperature distortion increased from 27.8 percent on the minimum compressor operating line to 33.5 percent near the compressor surge line (Fig. 10a).

For a constant corrected compressor airflow of 1.60 lbm/sec, the reheat nozzle entrance pressure distortion decreased from 9.5 percent on the minimum compressor operating line to 1.5 percent near the compressor surge line. The reheat nozzle entrance temperature distortion decreased from 35.1 percent on the minimum compressor operating line to 18.1 percent near the compressor surge line (Fig. 10b).

4.3 NOZZLE PERFORMANCE

In compliance with General Electric Test Plan (Ref. 4), nozzle performance was obtained along the nominal dry and reheat compressor operating lines (Fig. 11) at the following simulated flight conditions:

Mach Number	Altitude, ft
0.6	12,700
0.8	21,400
0.9	24,800
1.2	34,200
1.5	43,700

15

The dry and reheat nozzle thrust and nozzle flow coefficients are compared with predicted values in Fig. 12 as a function of nozzle pressure ratio and simulated flight Mach number. At nozzle pressure ratios above 3.0, the indicated dry nozzle thrust coefficient (Fig. 12a) ranged from approximately 0.97 to 1.01 and was from 0.8 to 1.5 percent higher than predicted. The average dry nozzle flow coefficient (Fig. 12a) was 0.948 (0.6 percent higher than the predicted value of 0.942) over the range of nozzle pressure ratios investigated.

The reheat nozzle thrust coefficient is shown in Fig. 12b. For nozzle pressure ratios above 3.0, the indicated nozzle thrust coefficient ranged from approximately 0.98 to 1.02 and was from 4.1 to 3.1 percent higher than predicted. The average reheat nozzle flow coefficient (Fig. 12b) was 0.987 (0.7 percent higher than the predicted value of 0.980) over the range of nozzle pressure ratios investigated.

4.4 OPERATIONAL EXPERIENCES

After eight hours and three minutes of simulator powered time in the motor mode (solid mixer and dry nozzle), the nozzle entrance honeycomb flow straightener failed. The flow straightener was removed and testing to map the compressor performance was initiated.

After thirty hours and fifty-five minutes of powered time, the reheat mixer became detached from the simulator. The reheat nozzle entrance anti-distortion screens and the reheat nozzle entrance pressure/temperature rake were destroyed. A mixer retainer was installed to hold the mixer in place. New anti-distortion screens and a new pressure/temperature rake were installed in the reheat nozzle, and testing was resumed.

Thirty-nine hours and six minutes of powered time were accumulated on the simulator during this test program.

5.0 SUMMARY OF RESULTS

A test program was conducted on an engine propulsion simulator to (1) determine the compressor maps at inlet pressures of 7, 12, and 16 psia at an inlet temperature of 120°F with both dry and reheat mixer/nozzle configurations, (2) determine the dry and reheat nozzle entrance pressure and temperature distortion, and (3) determine nozzle airflow and thrust characteristics at simulated altitude/Mach number flight conditions of 12,700/0.6, 21,400/0.8, 24,800/0.9, 34,200/1.2, and 43,700/1.5 with both mixer/nozzle configurations. The test results are summarized as follows:

5.1 COMPRESSOR MAPPING

5.1.1 Dry Configuration

At an inlet pressure of 7 psia, inlet temperature of 120°F, and corrected airflow of 1.60 lbm/sec, the compressor pressure ratio increased from 2.68 (5.6 percent lower than predicted) on the minimum operating line to 3.28 (as predicted) at the surge line, resulting in a stability margin of 22.4 percent.

The stability margin at a corrected compressor inlet airflow of 1.60 lbm/sec was 23.4 and 25.5 percent for compressor inlet pressures of 12 and 16 psia, respectively.

5.1.2 Reheat Configuration

At an inlet pressure of 7 psia, inlet temperature of 120°F, and corrected airflow of 1.60 lbm/sec, the compressor pressure ratio increased from 2.09 (4.1 percent lower than predicted) on the minimum operating line to 3.28 (determined during compressor mapping with the dry mixer/nozzle configuration) at the surge line, resulting in a stability margin of 56.9 percent.

The stability margin at a corrected compressor inlet airflow of 1.60 lbm/sec was 58.1 percent for a compressor inlet pressure of 12 psia.

5.2 NOZZLE TEMPERATURE AND PRESSURE DISTORTION

5.2.1 Dry Configuration

For a constant corrected compressor airflow of 1.60 lbm/sec, the nozzle entrance temperature distortion increased from 27.8 percent on the minimum compressor operating line to 33.5 percent near the compressor surge line. The nozzle entrance pressure distortion was less than 2.0 percent over the range of corrected compressor airflows investigated.

5.2.2 Reheat Configuration

For a constant corrected compressor airflow of 1.60 lbm/sec, the nozzle entrance temperature distortion decreased from 35.1 percent on the minimum compressor operating line to 18.1 percent near the compressor surge line, and the nozzle pressure distortion decreased from 9.5 percent on the minimum compressor operating to 1.5 percent near the compressor surge line.

5.3 NOZZLE PERFORMANCE

5.3.1 Nozzle Thrust Coefficient

For nozzle pressure ratios above 3.0, the dry nozzle thrust coefficient ranged from 0.97 to 1.01 and was from 0.8 to 1.5 percent higher than predicted. The reheat nozzle thrust coefficient ranged from 0.98 to 1.02 and was from 4.1 to 3.1 percent higher than predicted.

5.3.2 Nozzle Flow Coefficient

The dry nozzle flow coefficient was 0.948 (0.6 percent higher than predicted) and the reheat nozzle flow coefficient was 0.987 (0.7 percent higher than predicted) over the range of nozzle pressure ratios investigated.

5.4 OPERATIONAL EXPERIENCES

After eight hours and three minutes of simulator powered time in the motor mode, the nozzle entrance honeycomb flow straightener failed. The flow straightener was removed, and testing to map the compressor performance was initiated.

After thirty hours and fifty-five minutes of powered time, the reheat mixer became detached from the simulator. The reheat nozzle entrance anti-distortion screens and the reheat nozzle entrance pressure/temperature rake were destroyed. A new mixer with a retainer, new anti-distortion screens, and a new pressure/temperature rake were installed and testing was resumed.

Thirty-nine hours and six minutes of powered time were accumulated on the simulator during this test program.
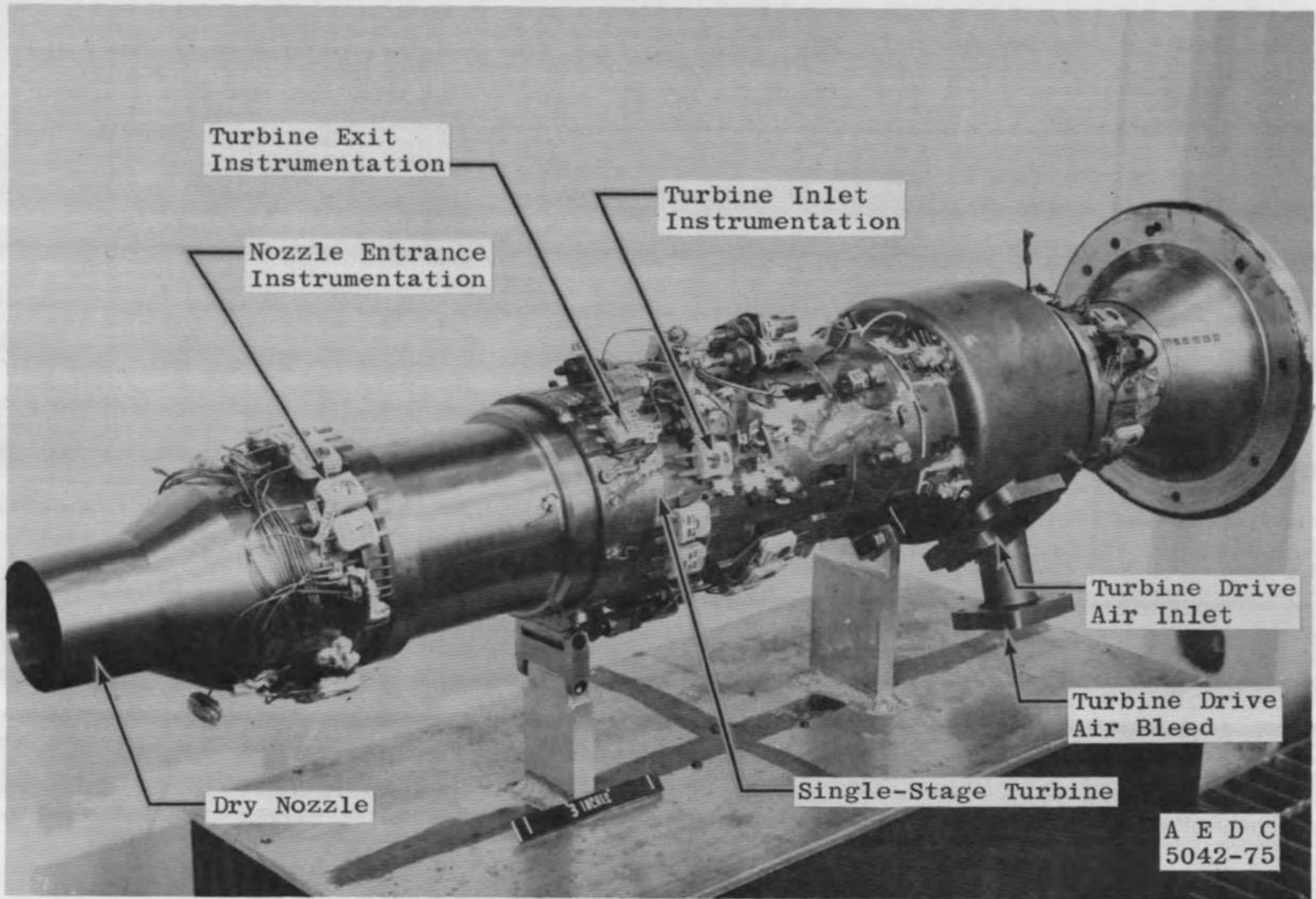
REFERENCES

1. Anderson, R. M., Laich, M. S., and Eigenmann, M. F. "Multimission Turbine Engine Propulsion Simulator Application Study." AFAPL-TR-72-107, November 1972.

2. Darlington, C. R., Brooksbank, R. M., and Brooks, J. O. "Component Performance and Stability Characteristics of an Engine Propulsion Simulator with Uniform and Distorted Pressure Profiles at Reynolds Number Indices of 0.39, 0.78, and 0.91." AEDC-TR-73-172 (AD775996), March 1974.

3. Darlington, C. R., and Brooks, J. O. "Performance of an Engine Propulsion Simulator and Control System at Sea-Level-Static Conditions." AEDC-TR-75-18 (ADB002520L), February 1975.
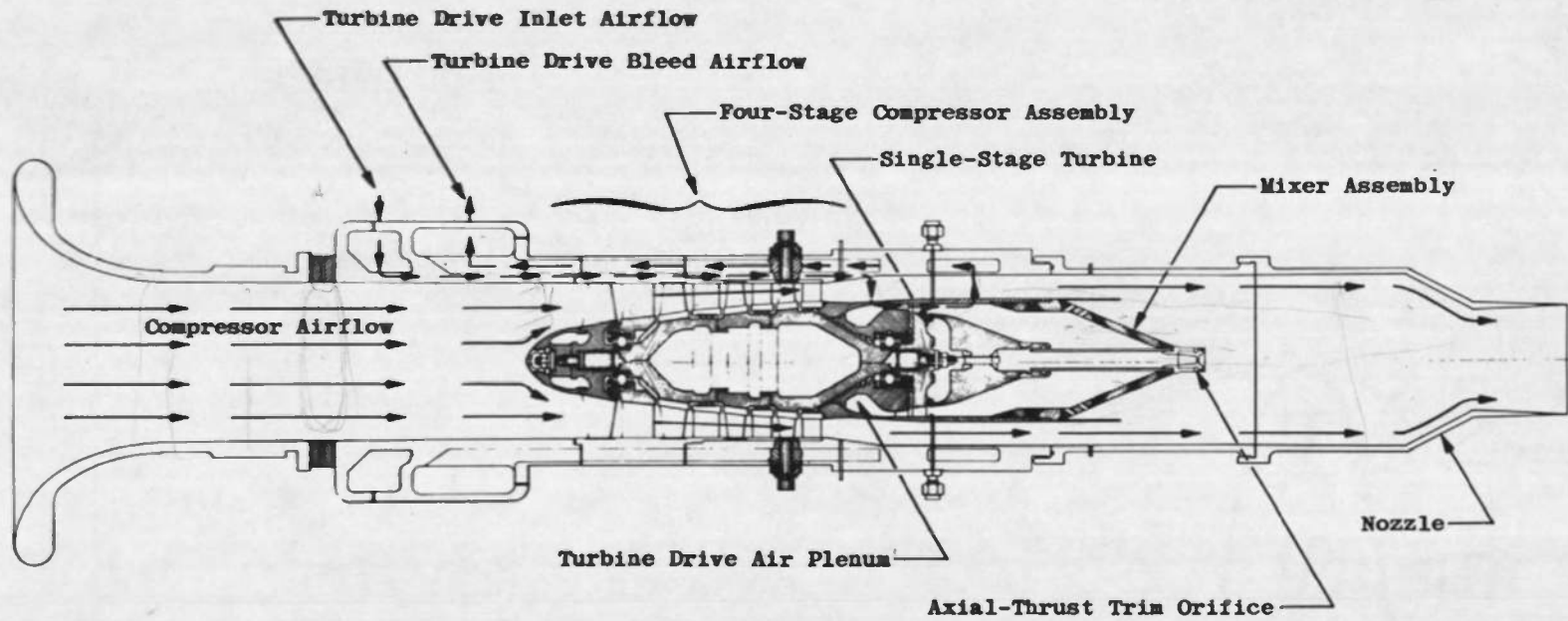
4. Delaney, B. R., Ruegg, R. G., and West, H. "Pre-Test Report for Calibration of SN 002/2 or SN 003/1 Propulsion Simulator in R2C4 Test Cell of ETF, AEDC." GE-TM-75-121, February 1975.

5. Delaney, B. R., West, H., and Prather, J. G. "Multi-Mission Turbine Engine Propulsion Simulator Users Console." AFAPL-TR-73-25, Volumes I and II, May 1973.

6. Owens, C. L. "Capabilities of the ESF Instrument Branch." AEDC-TR-67-18 (AD648707), March 1967.

7. Johnson, Robert C. "Real Gas Effects in Critical-Flow through Nozzles and Tabulated Thermodynamic Properties." NASA TN D-2565, Jamuary 1965.

8. Johnson, Robert C. "Real Gas Effects in Critical-Flow through Nozzles and Thermodynamic Properties of Nitrogen and Helium at Pressures to 300×10^5 Newtons per Square Meter (Approx. 300 Atm.)." NASA SP-3046, 1968.
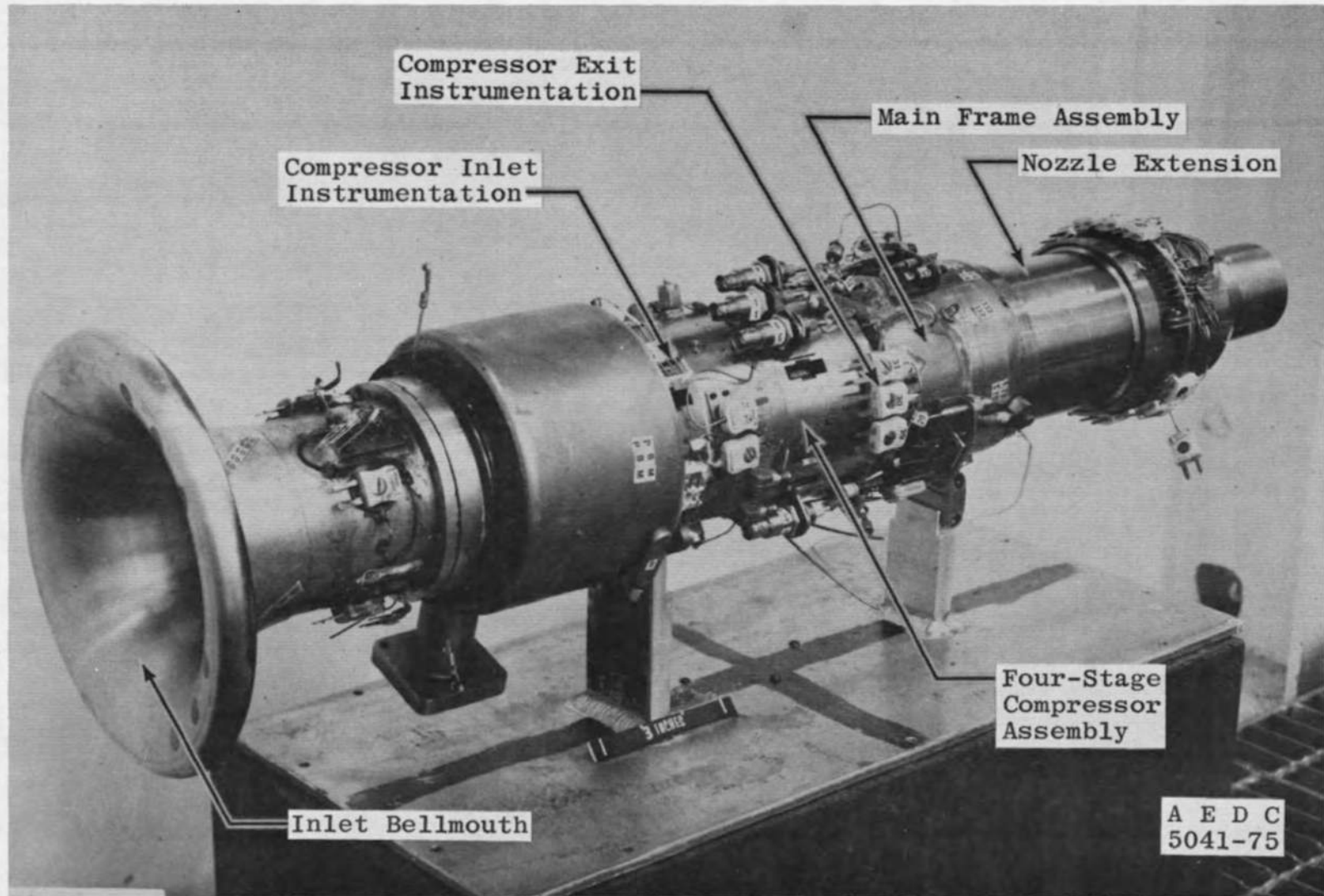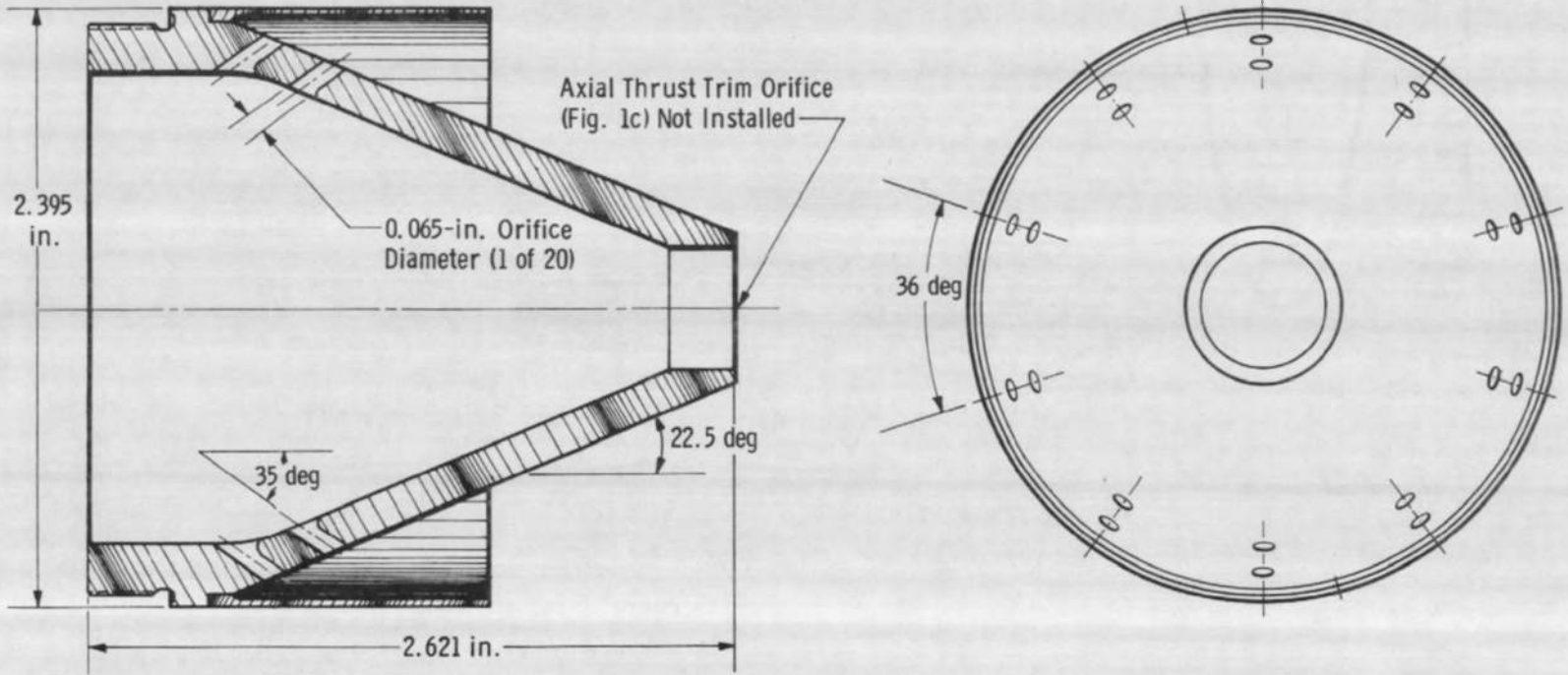
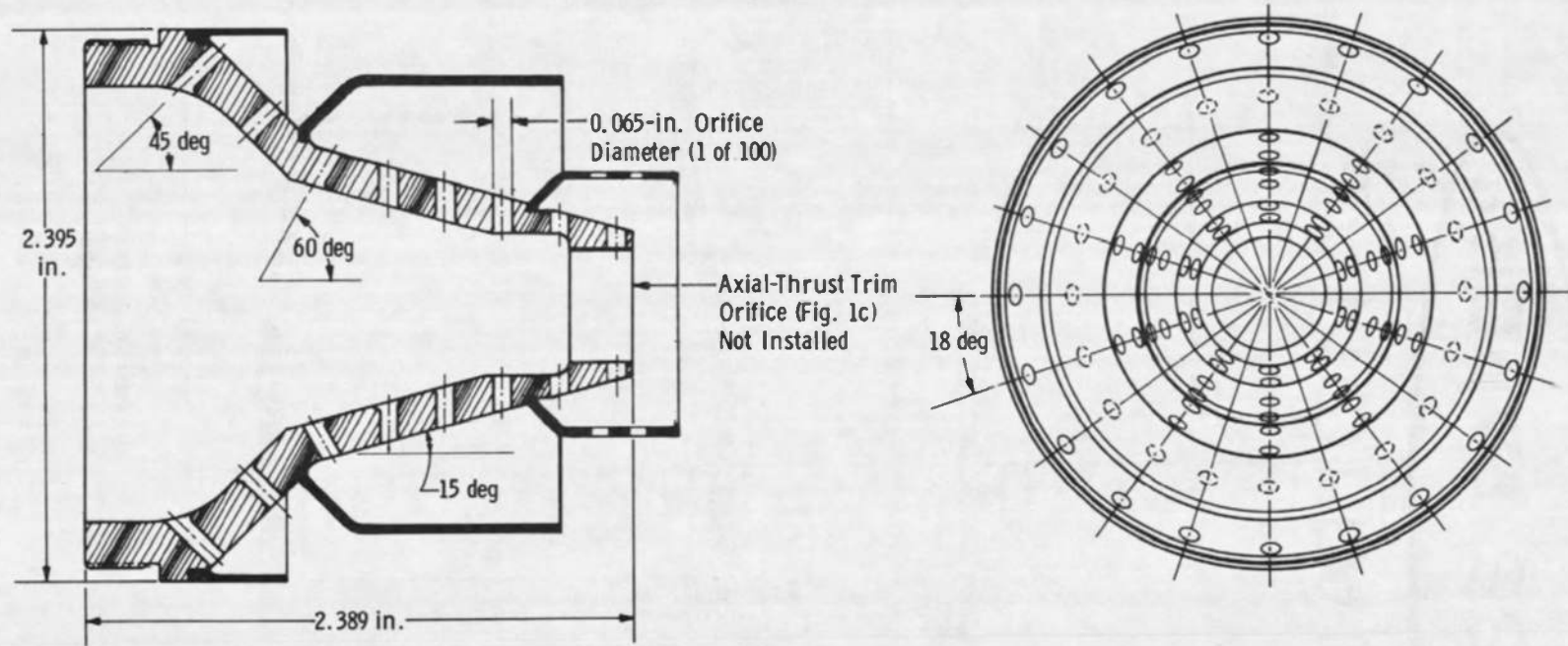a. Three-quarter front view
Figure 1. Engine propulsion simulator.

Turbine Exit
Instrumentation

Turbine Inlet
Instrumentation

Nozzle Entrance
Instrumentation

Turbine Drive
Air Inlet

Turbine Drive
Air Bleed

Dry Nozzle

Single-Stage Turbine

AEDC
5042-75

b. Three-quarter rear view
Figure 1. Continued.

Turbine Drive Inlet Airflow

Turbine Drive Bleed Airflow

Four-Stage Compressor Assembly

Single-Stage Turbine

Mixer Assembly

Compressor Airflow

Turbine Drive Air Plenum

Axial-Thrust Trim Orifice

Nozzle

c. Cross-sectional schematic
Figure 1. Continued.

Axial Thrust Trim Orifice
(Fig. 1c) Not Installed

0.065-in. Orifice
Diameter (1 of 20)

2.395
in.

36 deg

22.5 deg

35 deg

2.621 in.

d. Dry mixer
Figure 1. Continued.

0.065-in. Orifice
Diameter (1 of 100)

Axial-Thrust Trim
Orifice (Fig. 1c)
Not Installed

45 deg

60 deg

15 deg

18 deg

2.395 in.

2.389 in.

e. Reheat mixer
Figure 1. Continued.

Nozzle Entrance Anti-Distortion Screen

Station 7 Pressure/Temperature Rake

28 deg

3.290 in

4.000 in.

1.993 in.

2.115 in.

5.79 in.

f. Dry nozzle

9 deg

3.290 in.

4.000 in.

2.698 in.

3.294 in.

5.91 in.
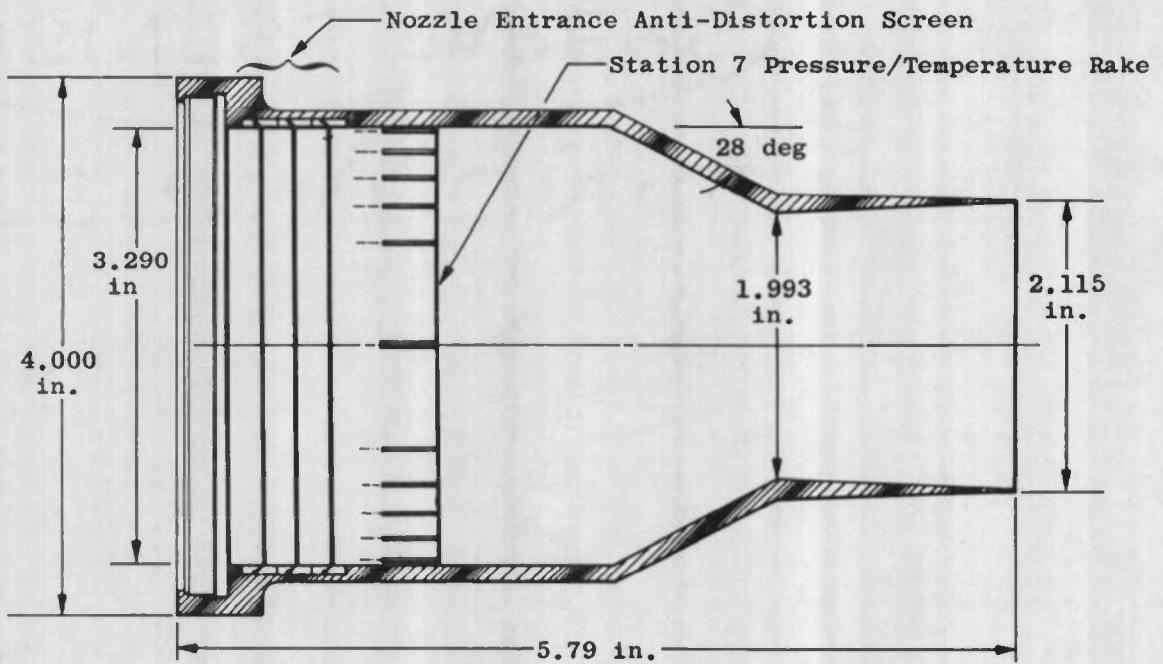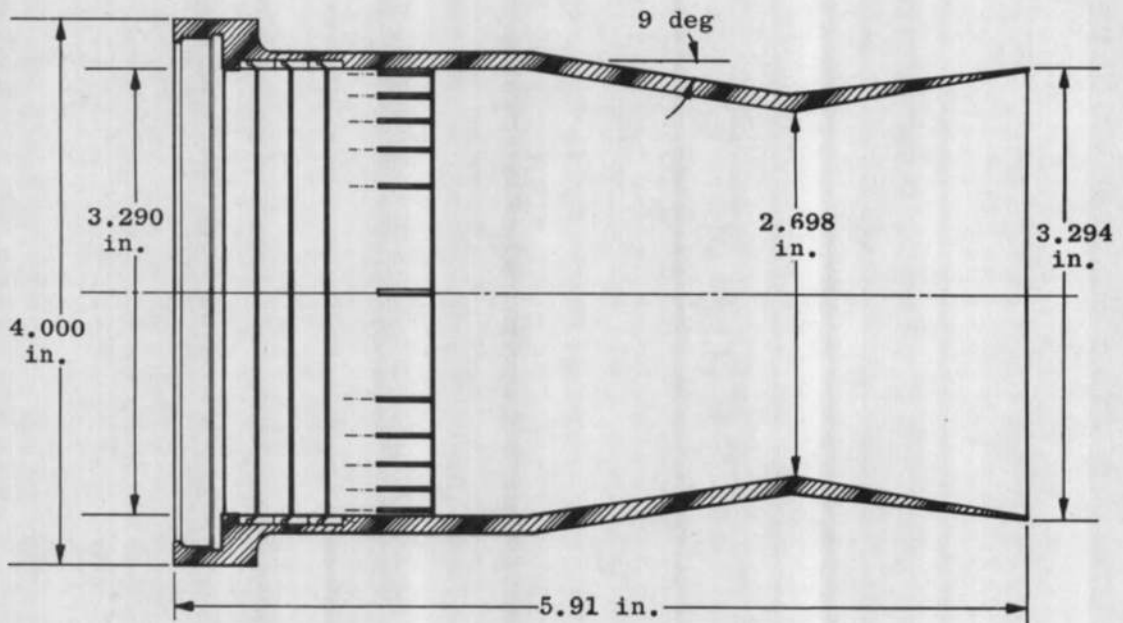
g. Reheat nozzle
Figure 1. Continued.
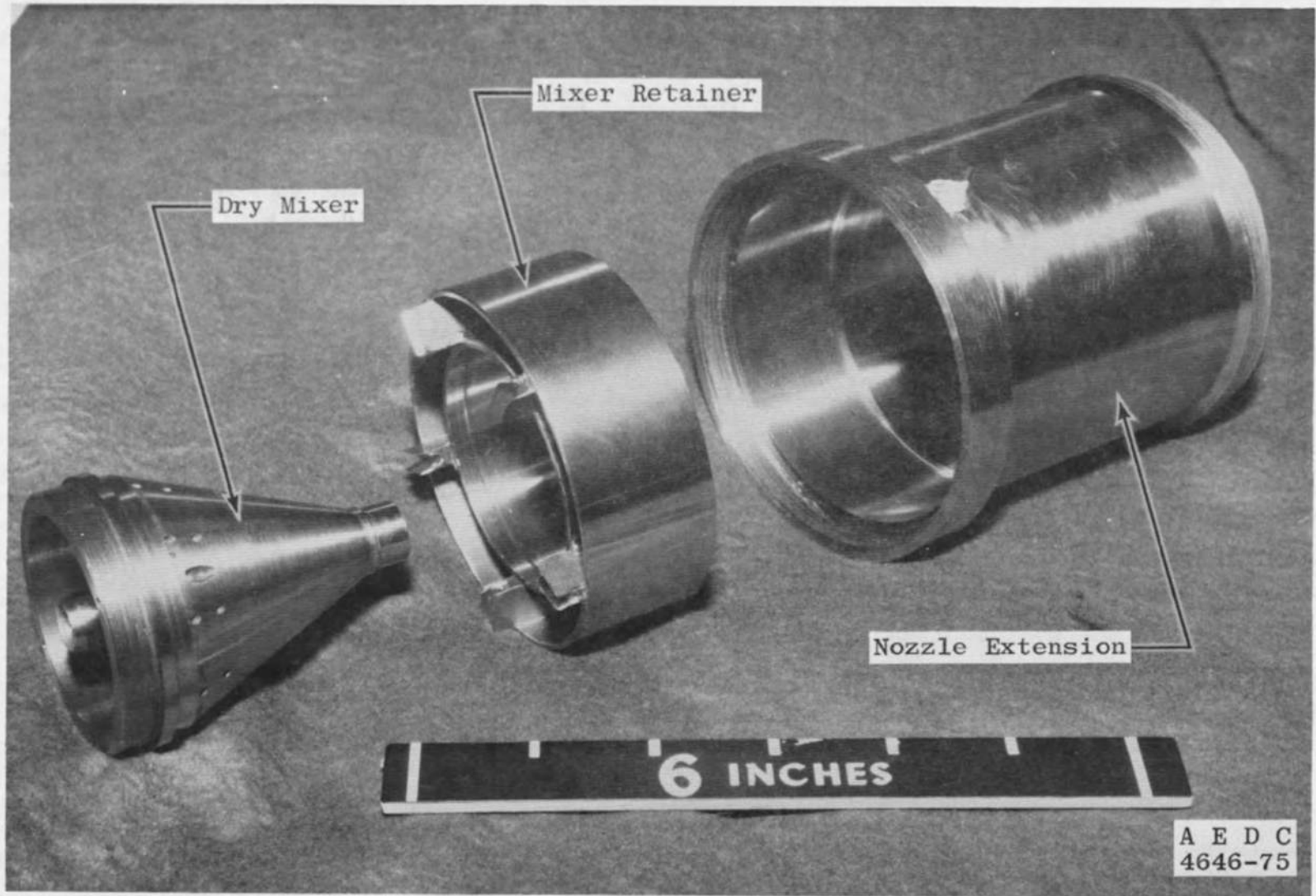
h. Mixer retainer
Figure 1. Concluded.
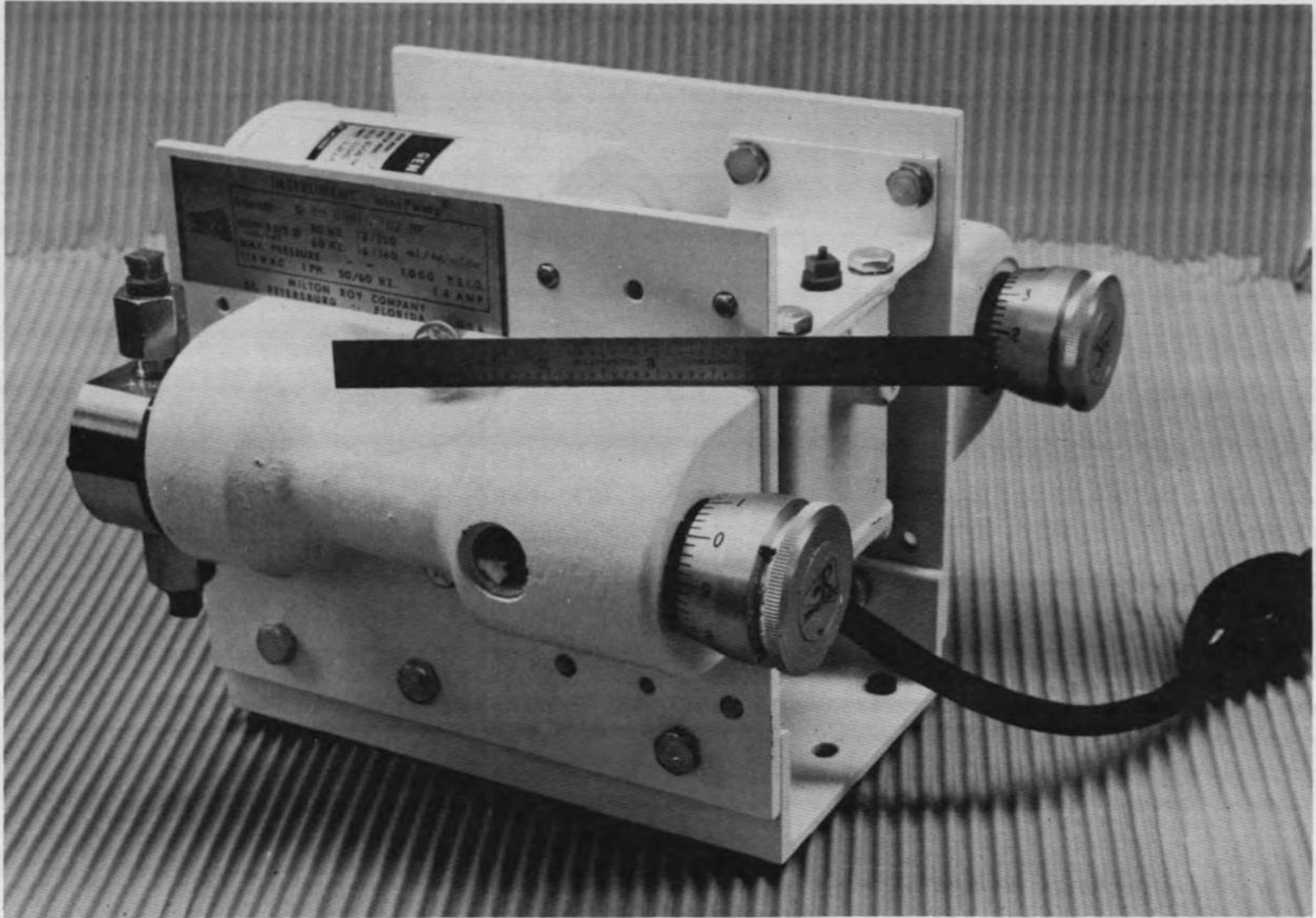
a. Mini-pump

Figure 2. Lube oil system.
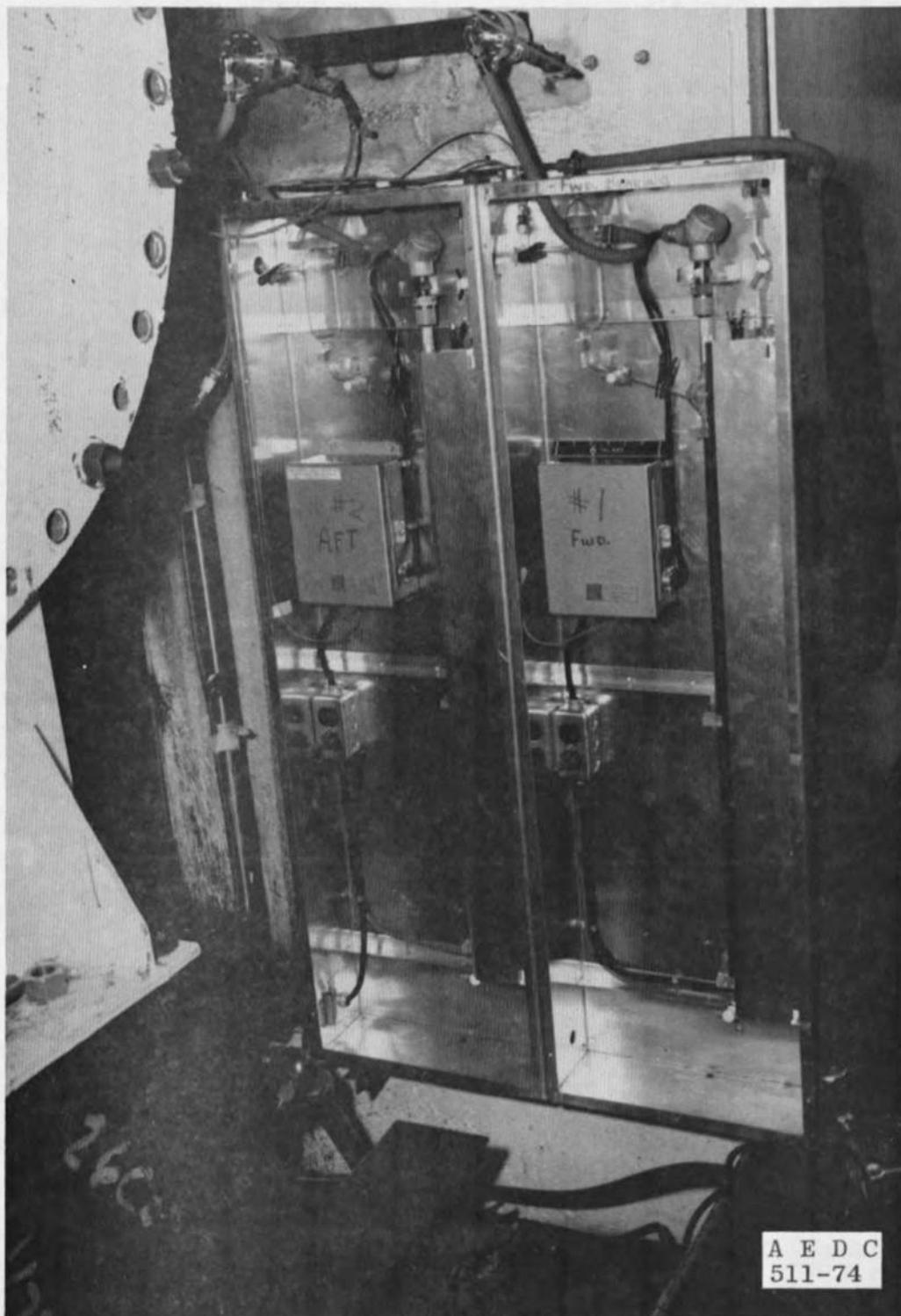
b. Oil scavenge system
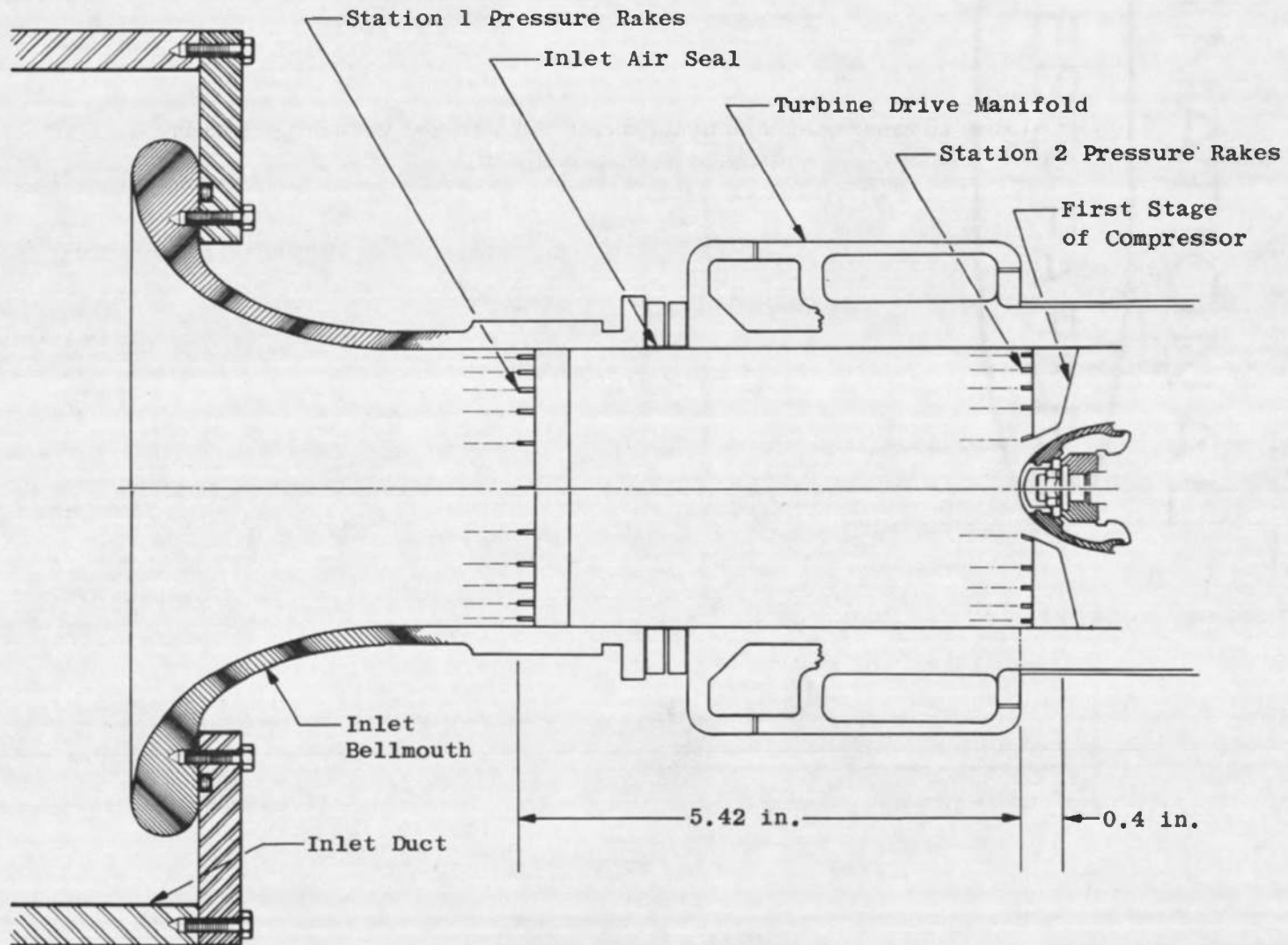Figure 2. Concluded.

Compressor Inlet Air-
Measuring Venturi

Thrust-Measuring System

Mount Assembly

Compressor Inlet
Control Valve

Test Cell

Exhaust Ducting

Flow-Straightening Screen

Simulator (See Fig. 3b for
Details of Inlet Configuration)

Inlet Ducting (10-in. diam)
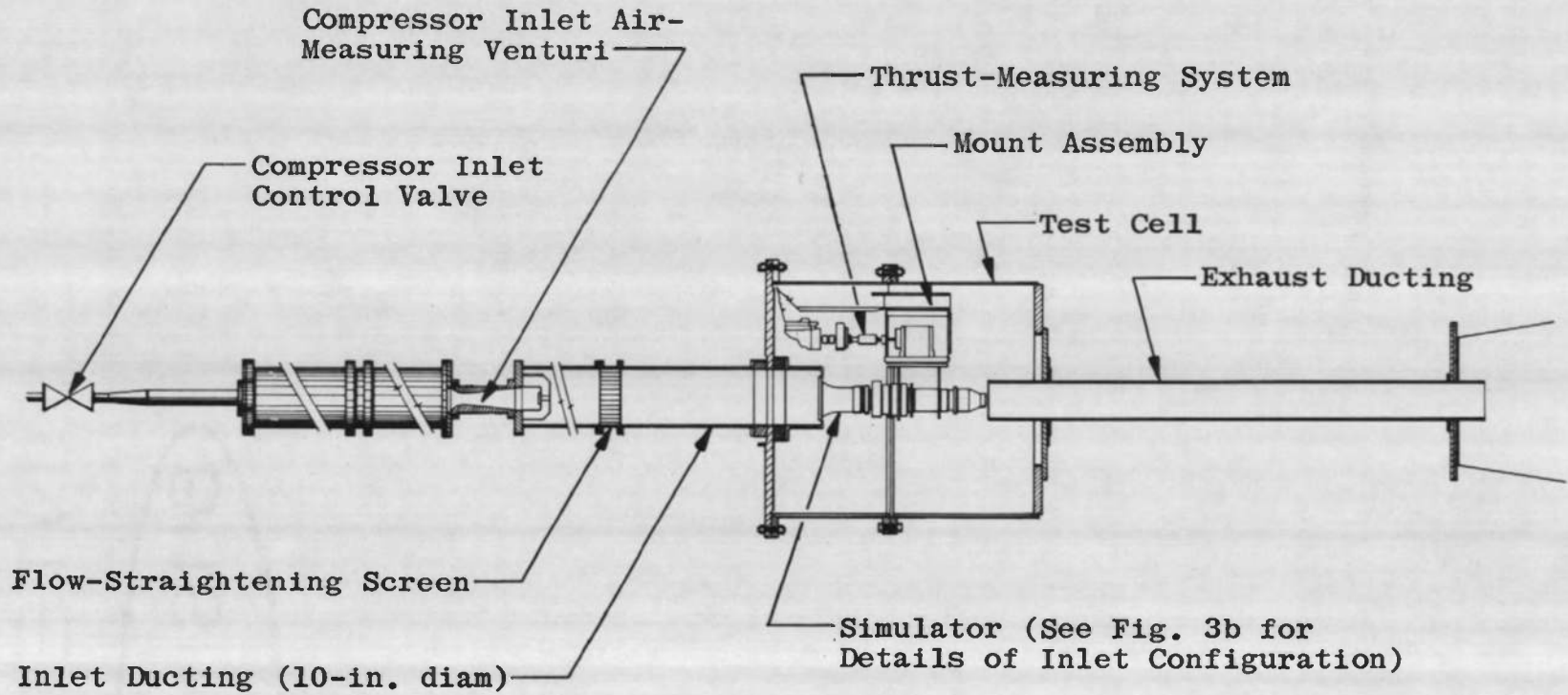
a. Cross-sectional schematic
Figure 3. Propulsion simulator test installation in Propulsion Research Area (R-2C-4).

Station 1 Pressure Rakes

Inlet Air Seal

Turbine Drive Manifold

Station 2 Pressure Rakes

First Stage of Compressor

Inlet Bellmouth

Inlet Duct

5.42 in.

0.4 in.

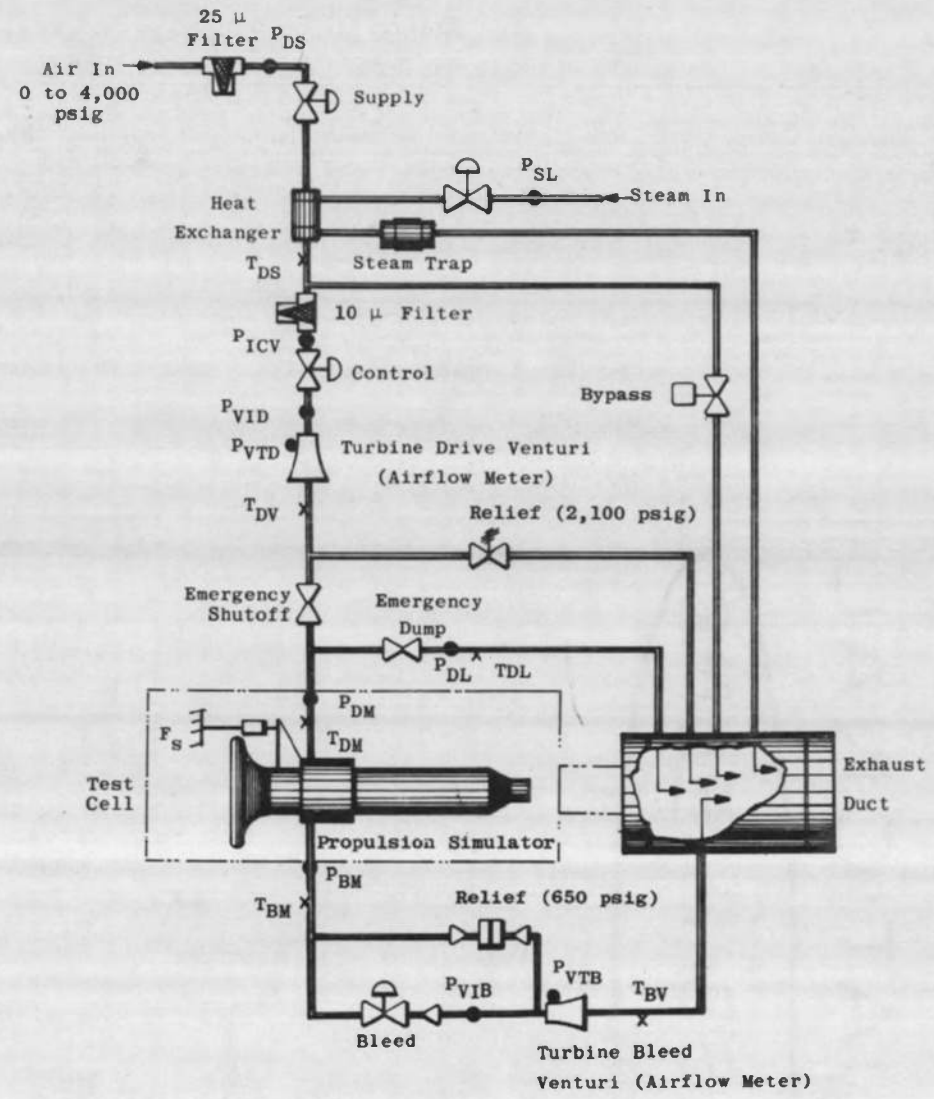b. Details of simulator inlet
Figure 3. Concluded.

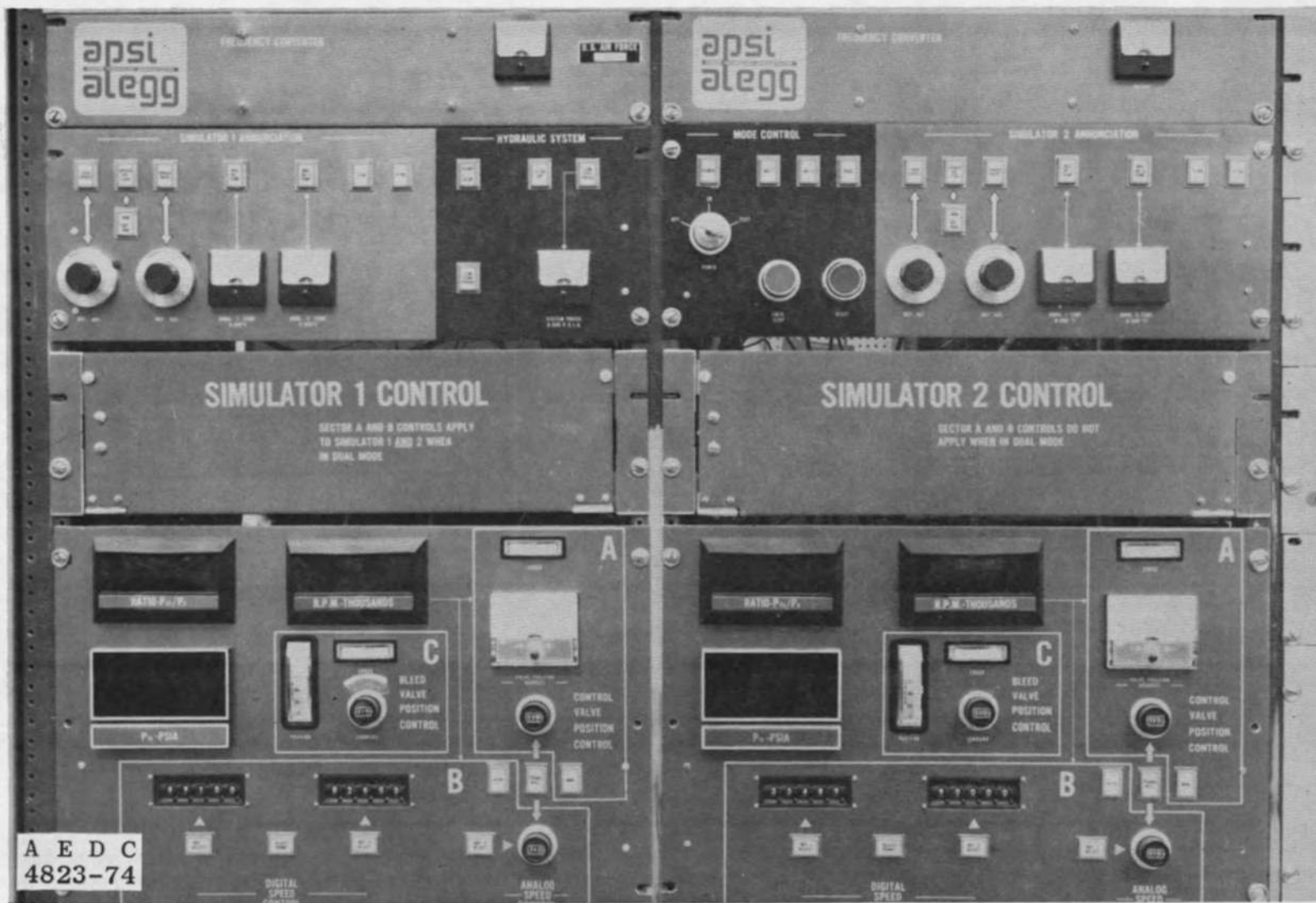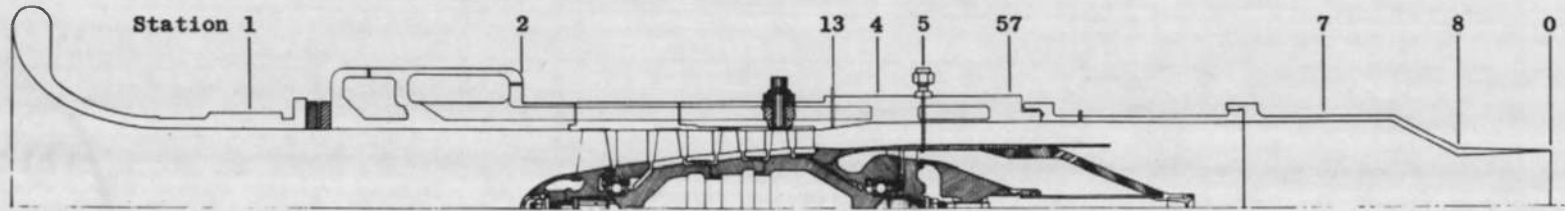Figure 4. Schematic of turbine drive air system.

Figure 5. Simulator control console.

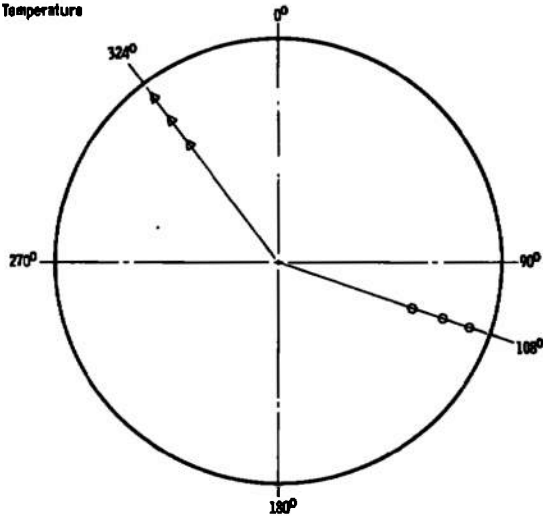| Station Parameter	Bellmouth	Compressor Inlet	Compressor Exit	Turbine Inlet	Turbine Exit	Mixer Entrance	Nozzle Entrance	Nozzle Throat	Nozzle Exit
	1	2	13	4	5	57	7	8	
Total Pressure	16	25	9	2	3		11		
Wall Static Pressure	4		3			1			
Total Temperature	5		6	2	4		11		
Dynamic Pressure		1	1						
Static Pressure									2

a. Station location
Figure 6. Propulsion simulator instrumentation.
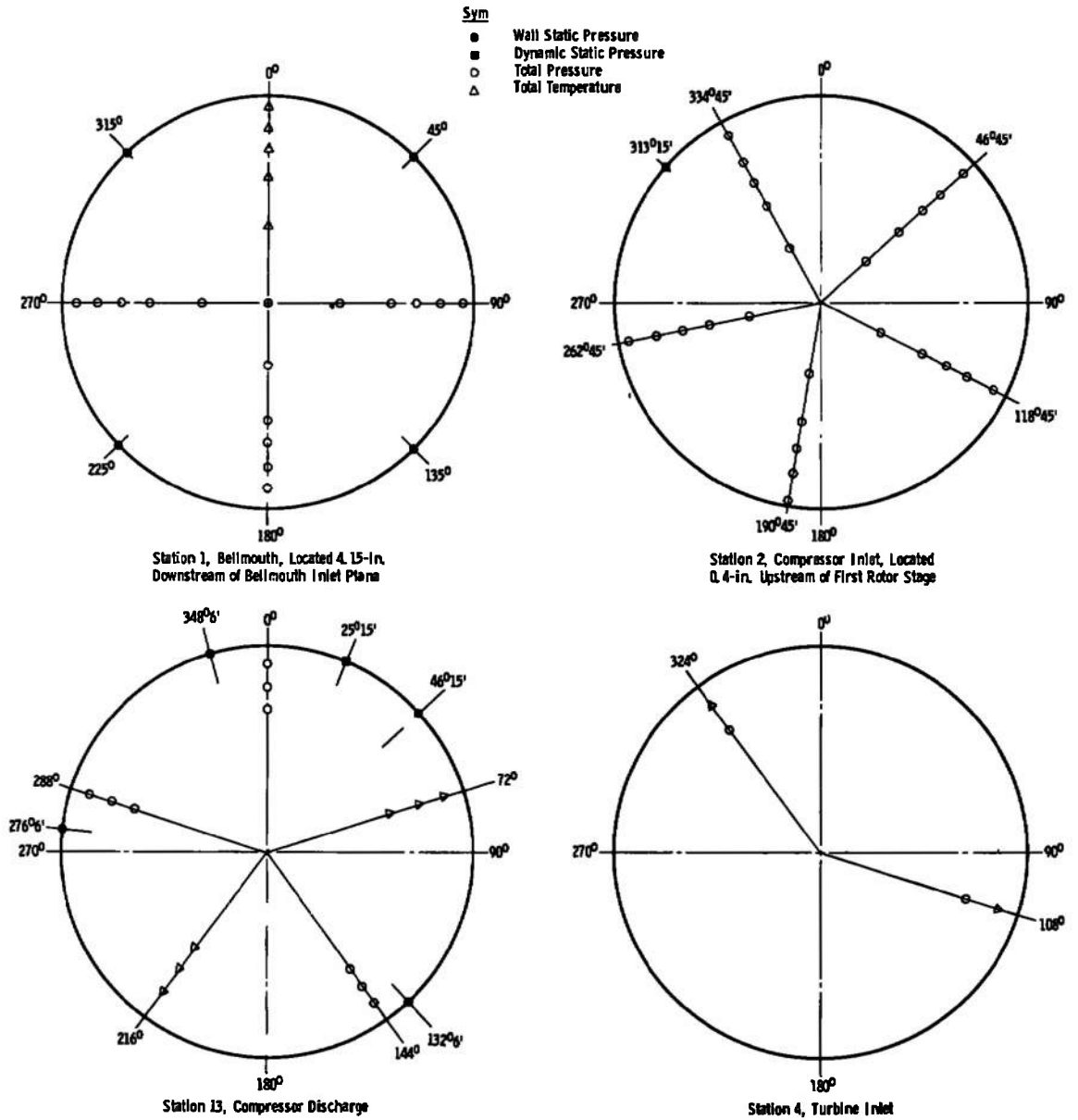
b. Instrumentation details (looking upstream)
Figure 6. Continued.
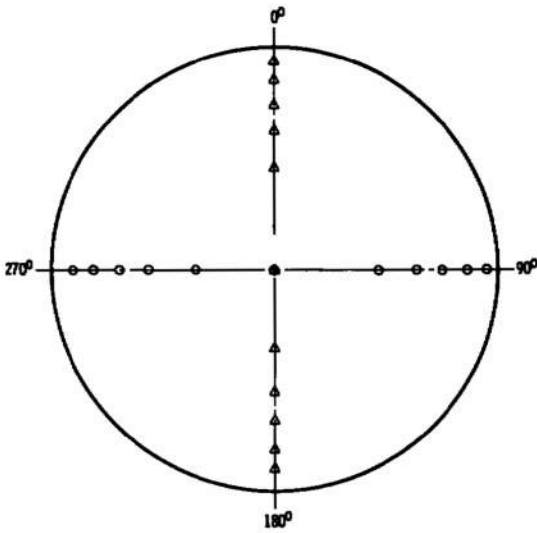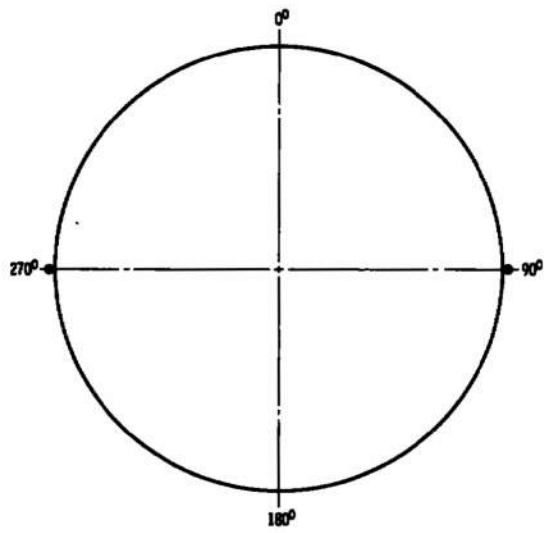
b. Concluded
Figure 6. Concluded.

Static Pressure ⟶ Increasing

Compressor
Discharge, PS$_{13}$

Compressor
Inlet, PS$_2$

First Indication
of Surge

Rotor Speed, Constant
Compressor Back Pressure, Increasing

| 0 | 25 | 50 | 75 | 100 | 125 | 150 | 175 | 200 |

Time, msec
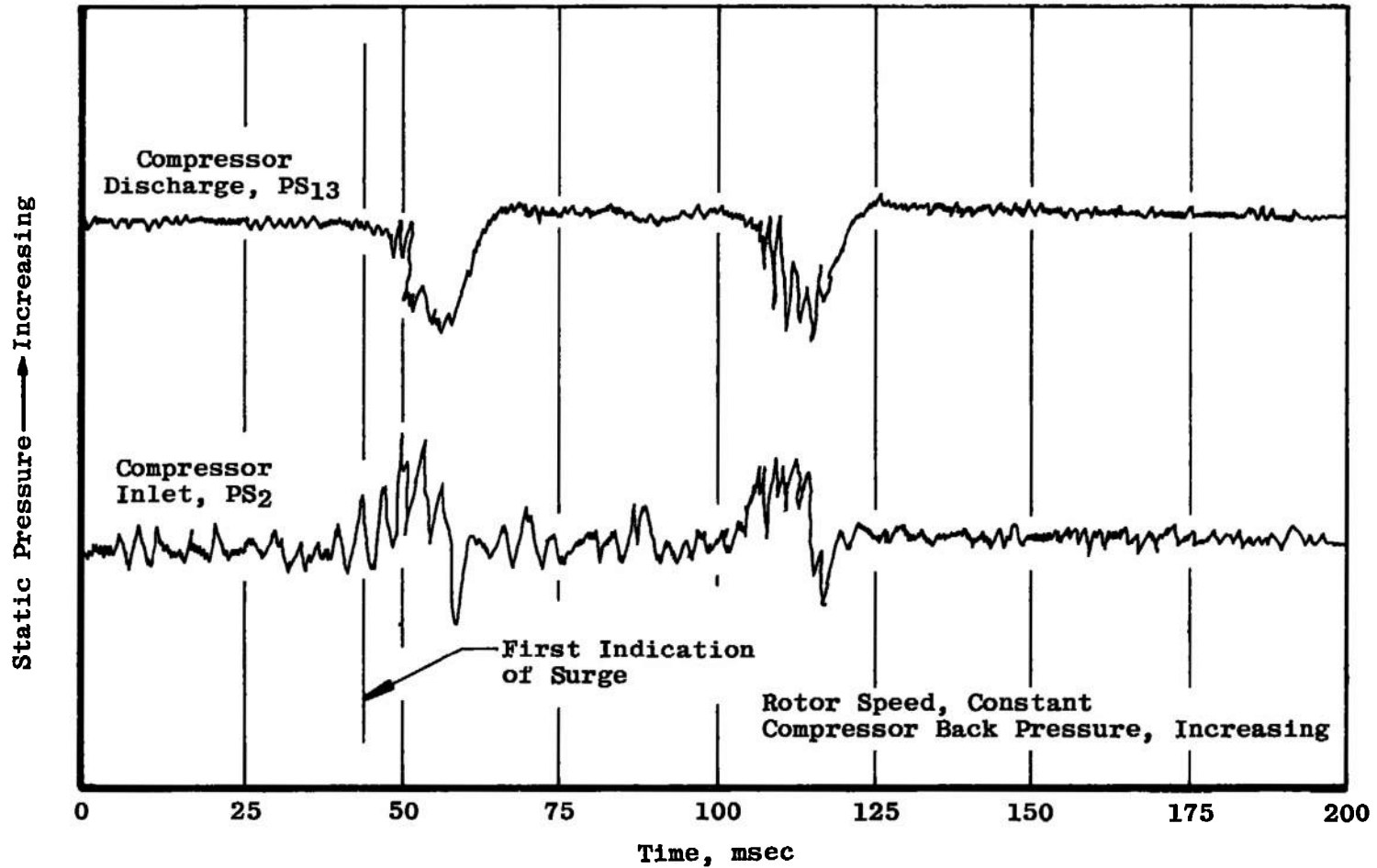
Figure 7. Typical transient pressures during incipient compressor surge.
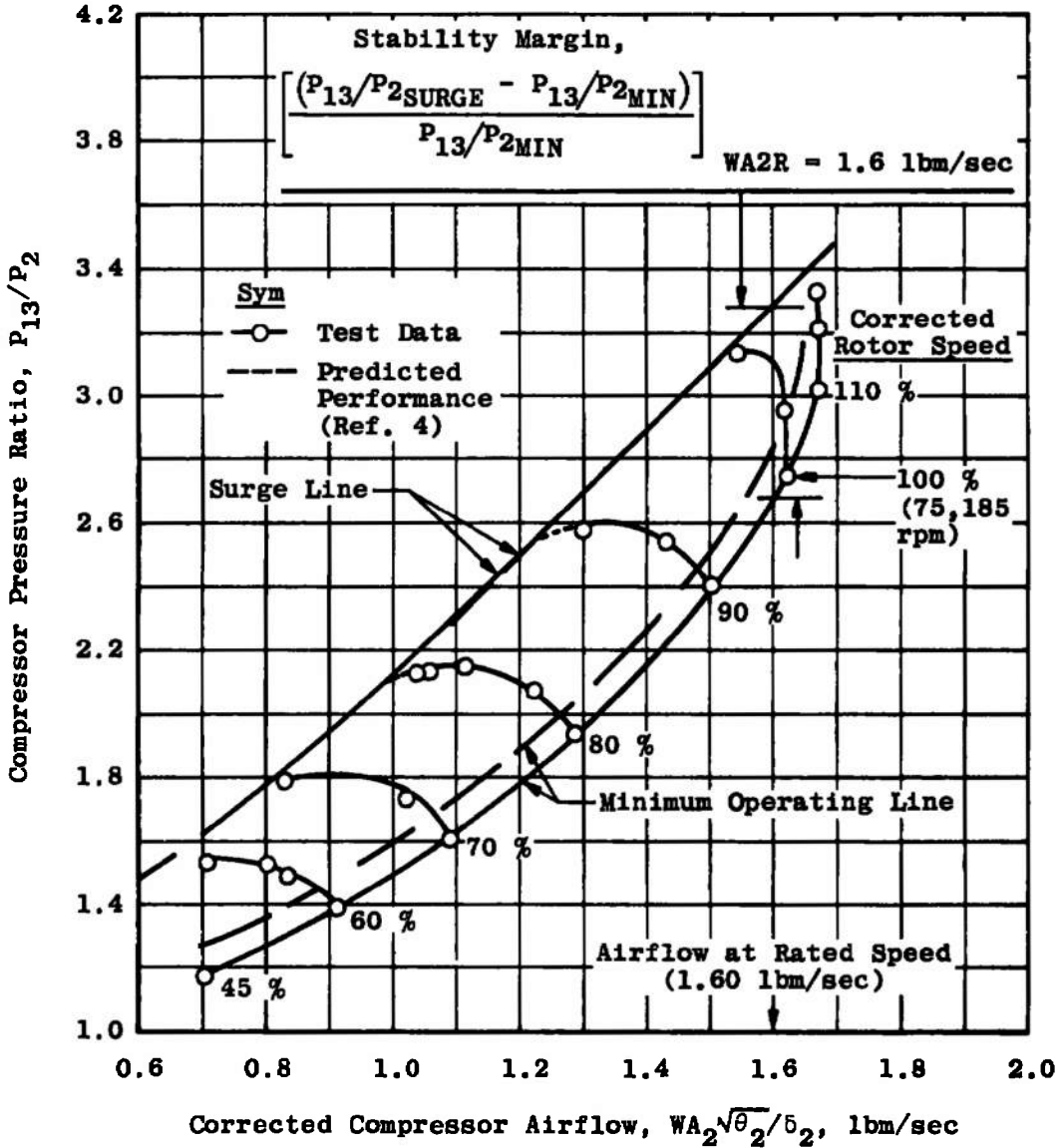
a. Compressor inlet pressure (P_2) = 7 psia

Figure 8. Compressor operating map with the dry nozzle configuration $(A_8 = 3.12 \text{ in.}^2, T_2 = 120°F)$.
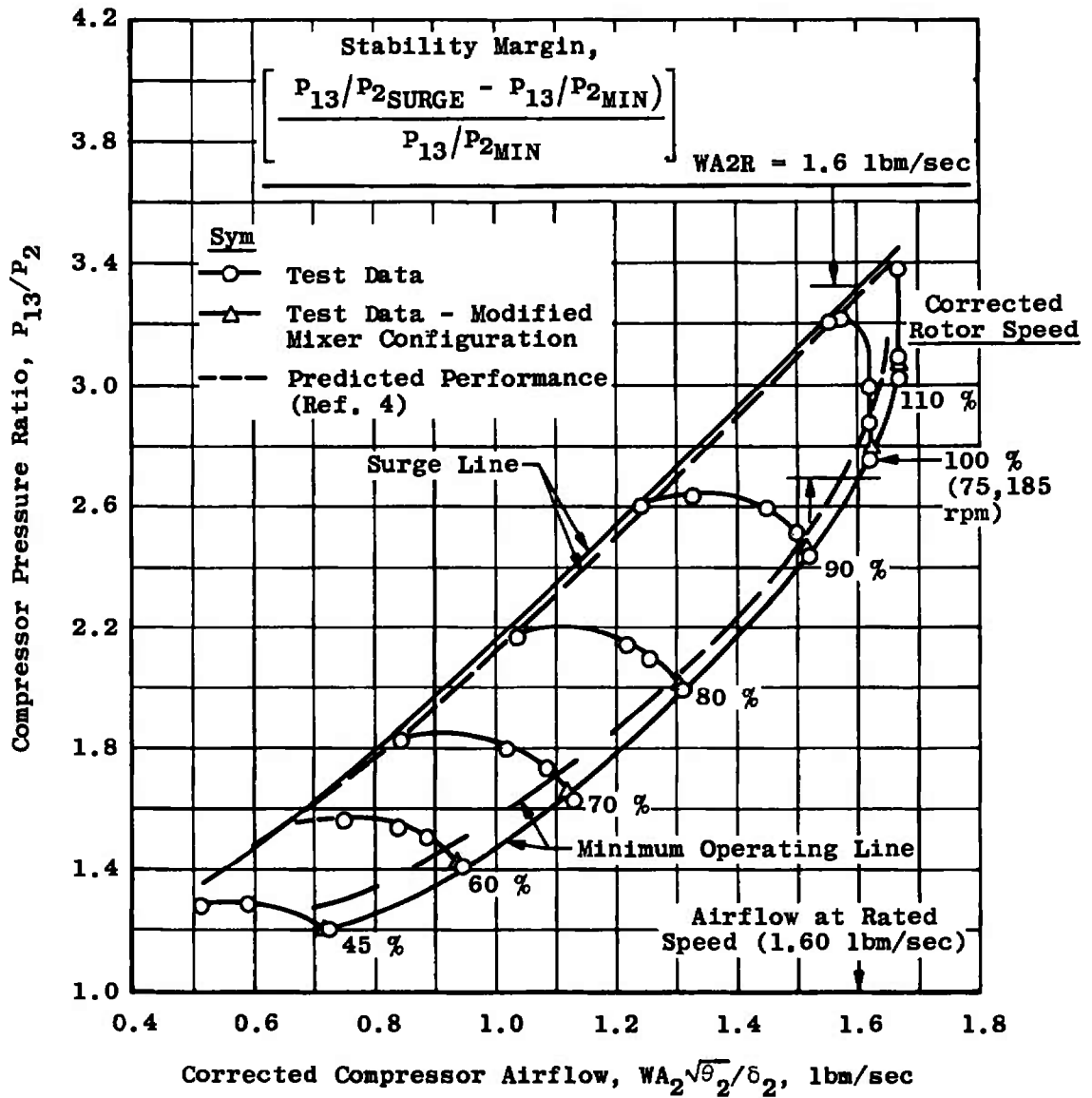
b. Compressor inlet pressure (P_2) = 12 psia
Figure 8. Continued.
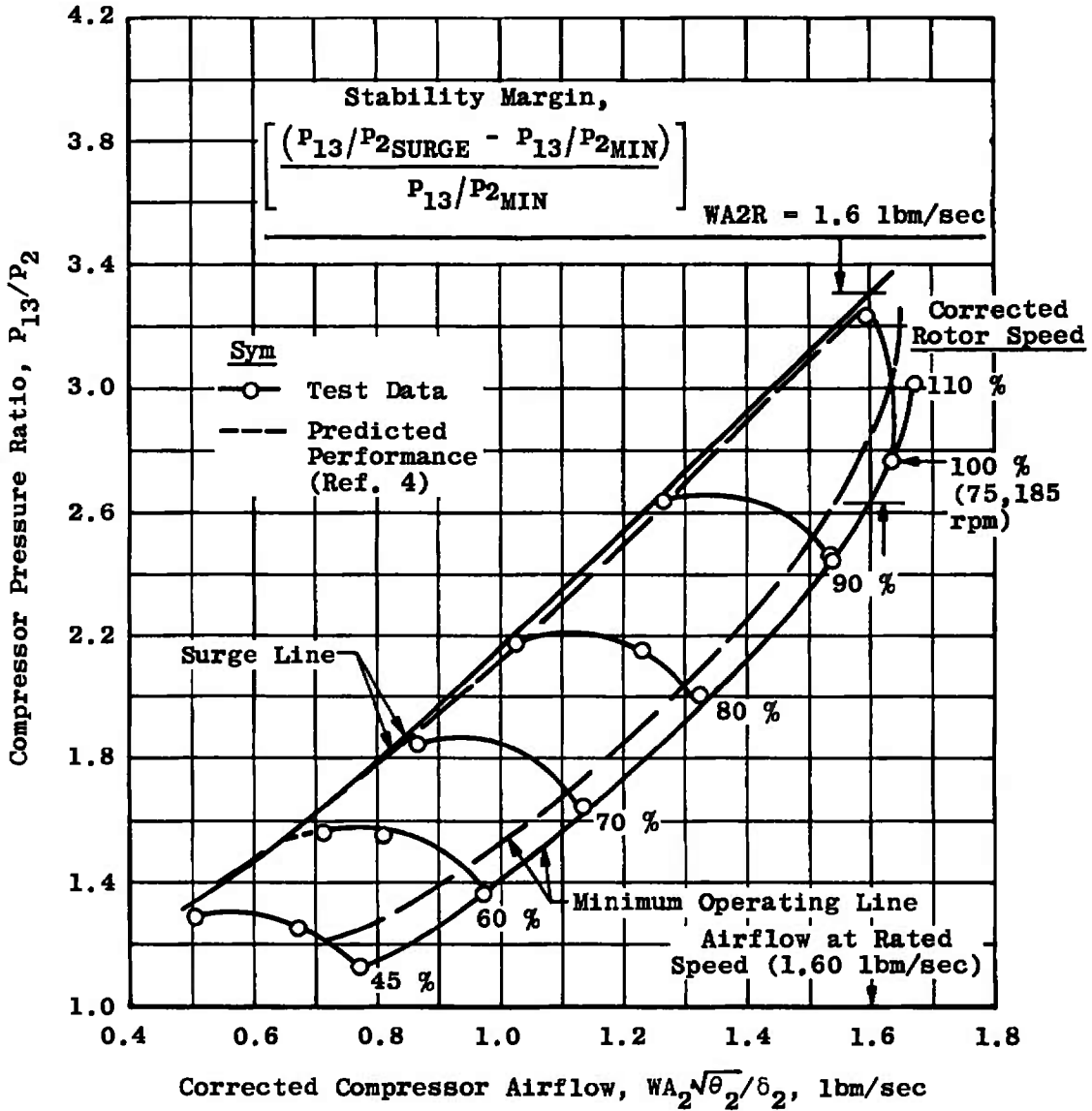
c. Compressor inlet pressure (P_2) = 16 psia
Figure 8. Concluded.
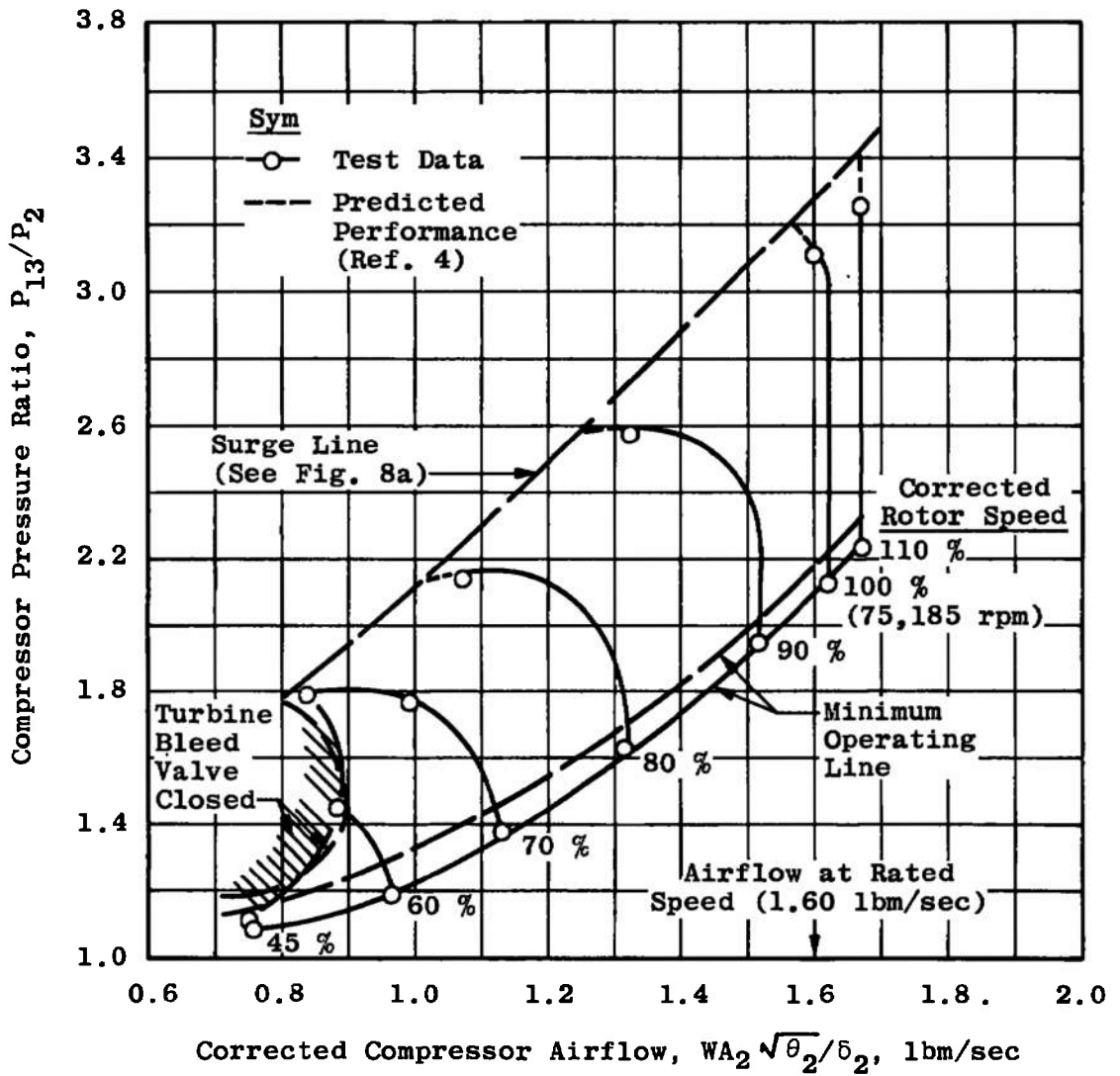
a. Compressor inlet pressure (P_2) = 7 psia

Figure 9. Compressor operating map with the reheat nozzle configuration (A_8 = 5.72 in.^{2}, T_2 = 120°F).
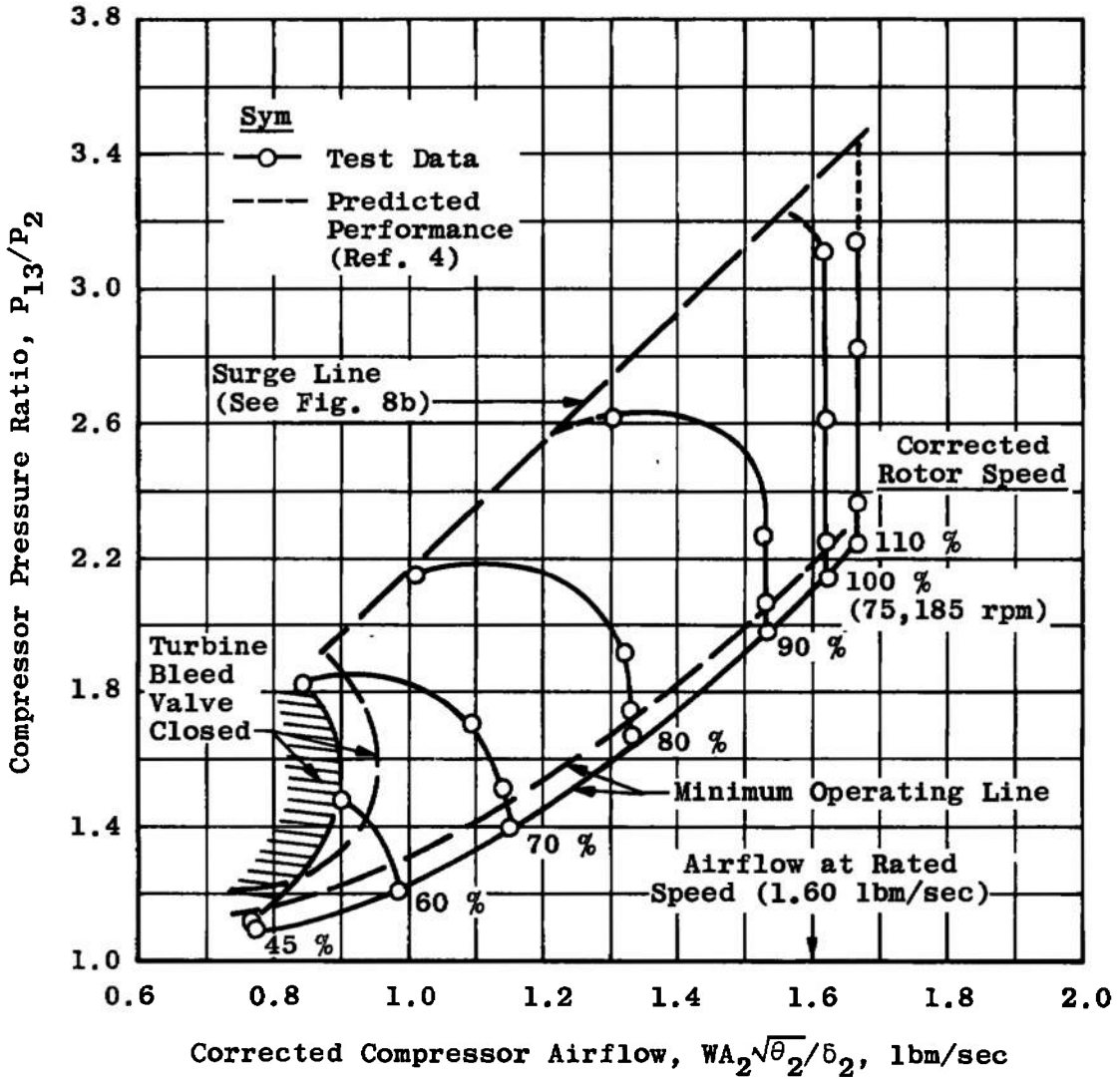
b. Compressor inlet pressure (P_2) = 12 psia
Figure 9. Continued.

Corrected Compressor Airflow, $WA_2\sqrt{\theta_2}/\delta_2$, lbm/sec
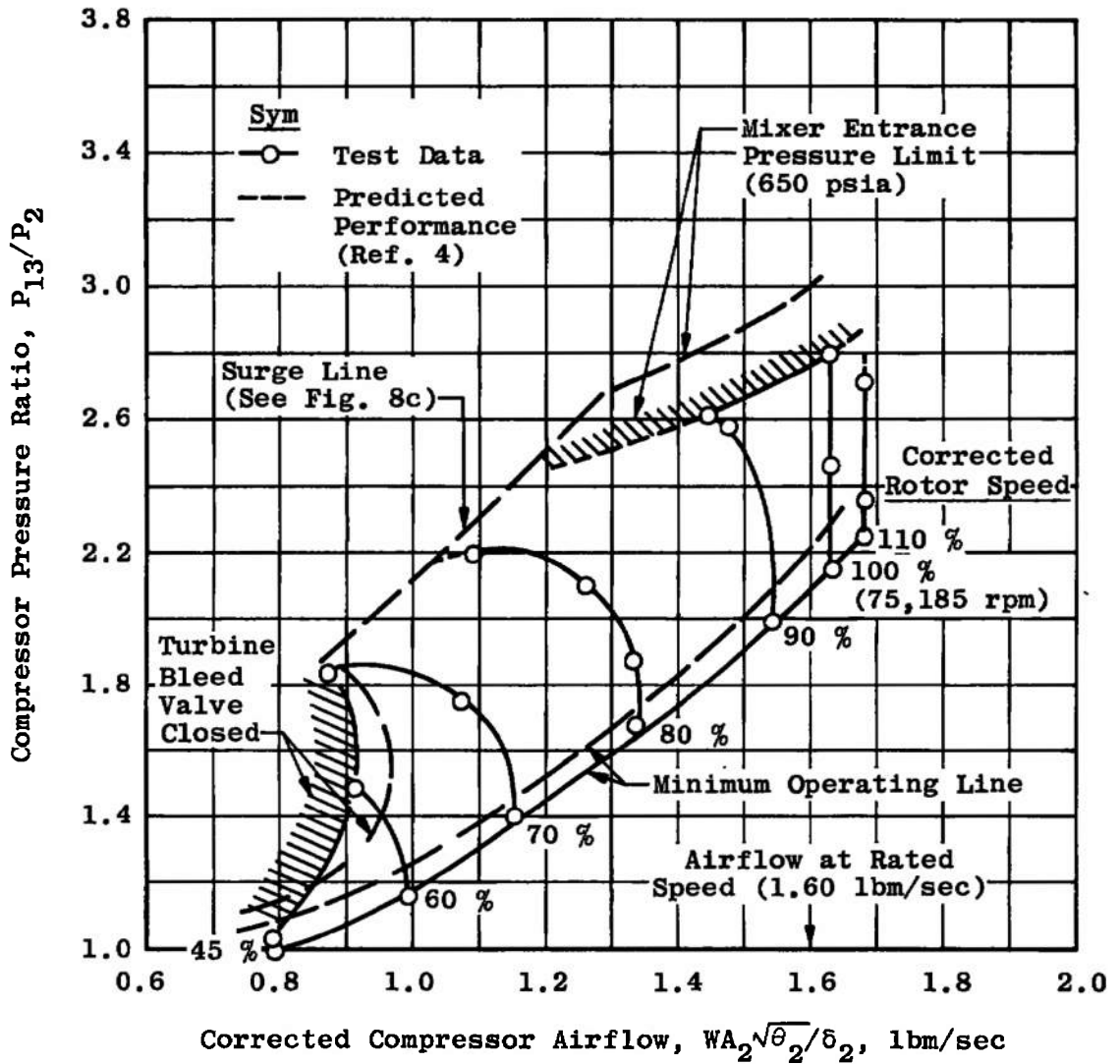
c. Compressor inlet pressure (P_2) = 16 psia
Figure 9. Concluded.
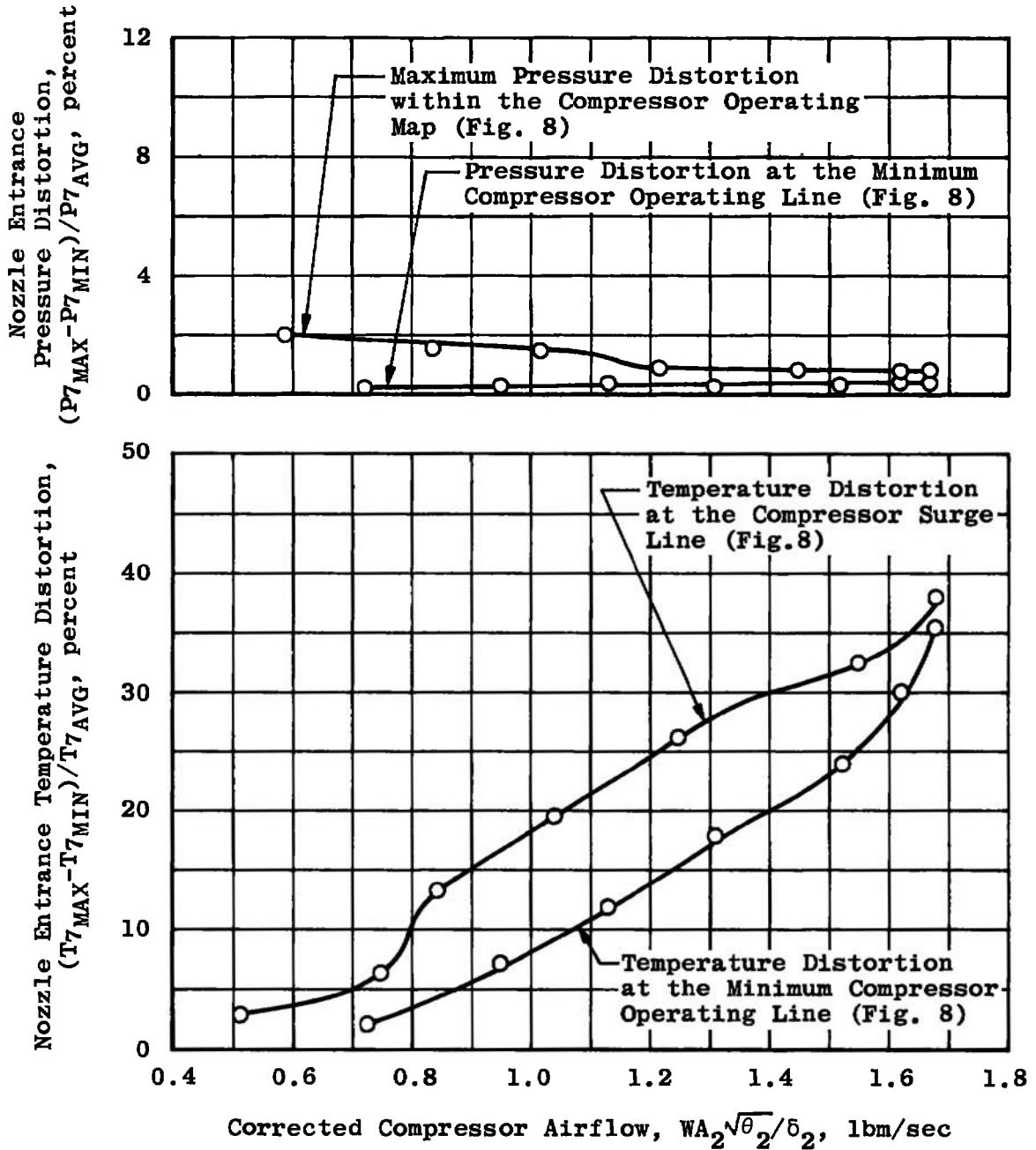
a. Dry configuration (A_8 = 3.12 in.^{2})

Figure 10. Nozzle entrance pressure and temperature distortion as a function of corrected compressor airflow.
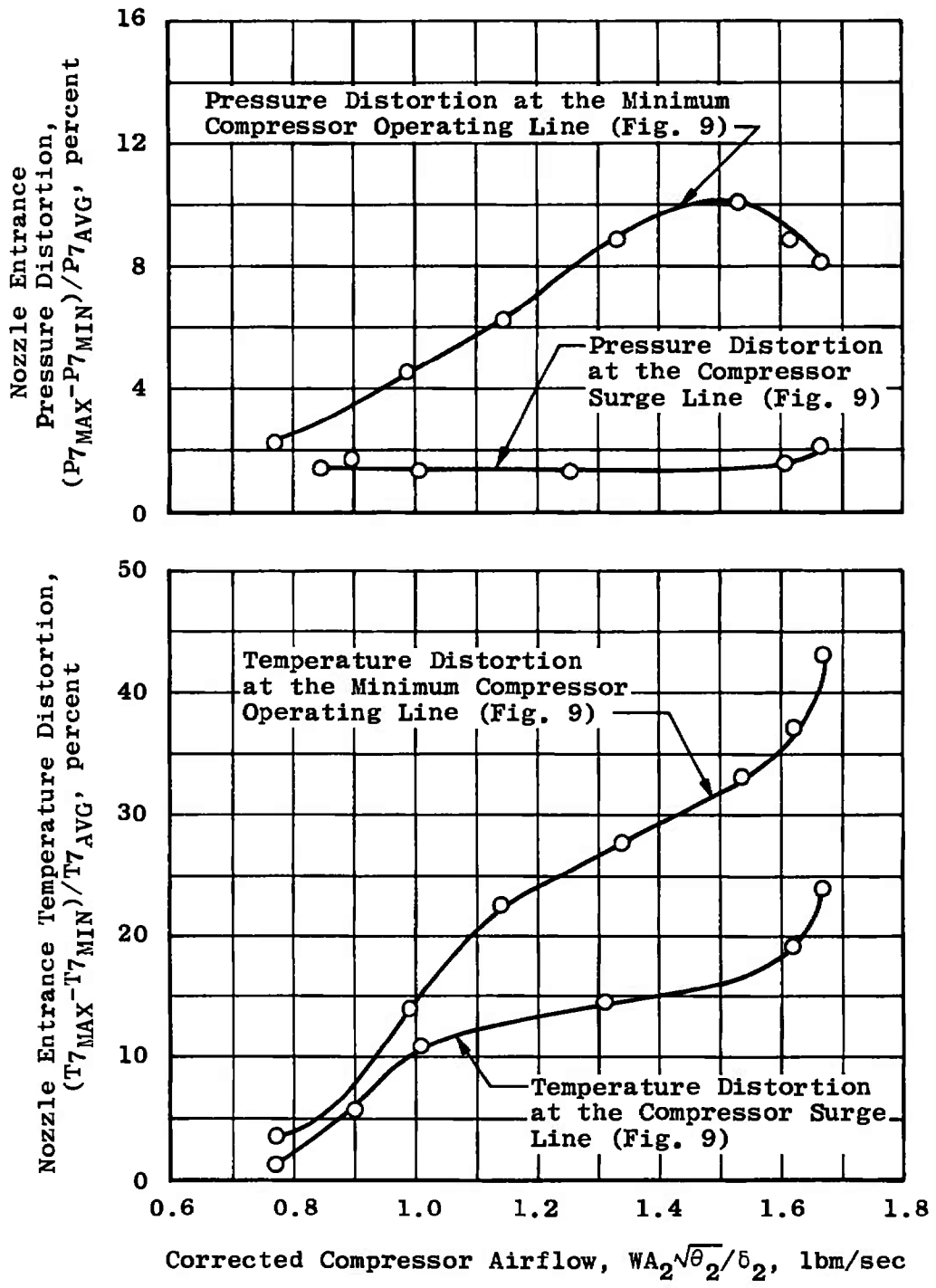
b. Reheat configuration (A_8 = 5.72 in.^{2})
Figure 10. Concluded.
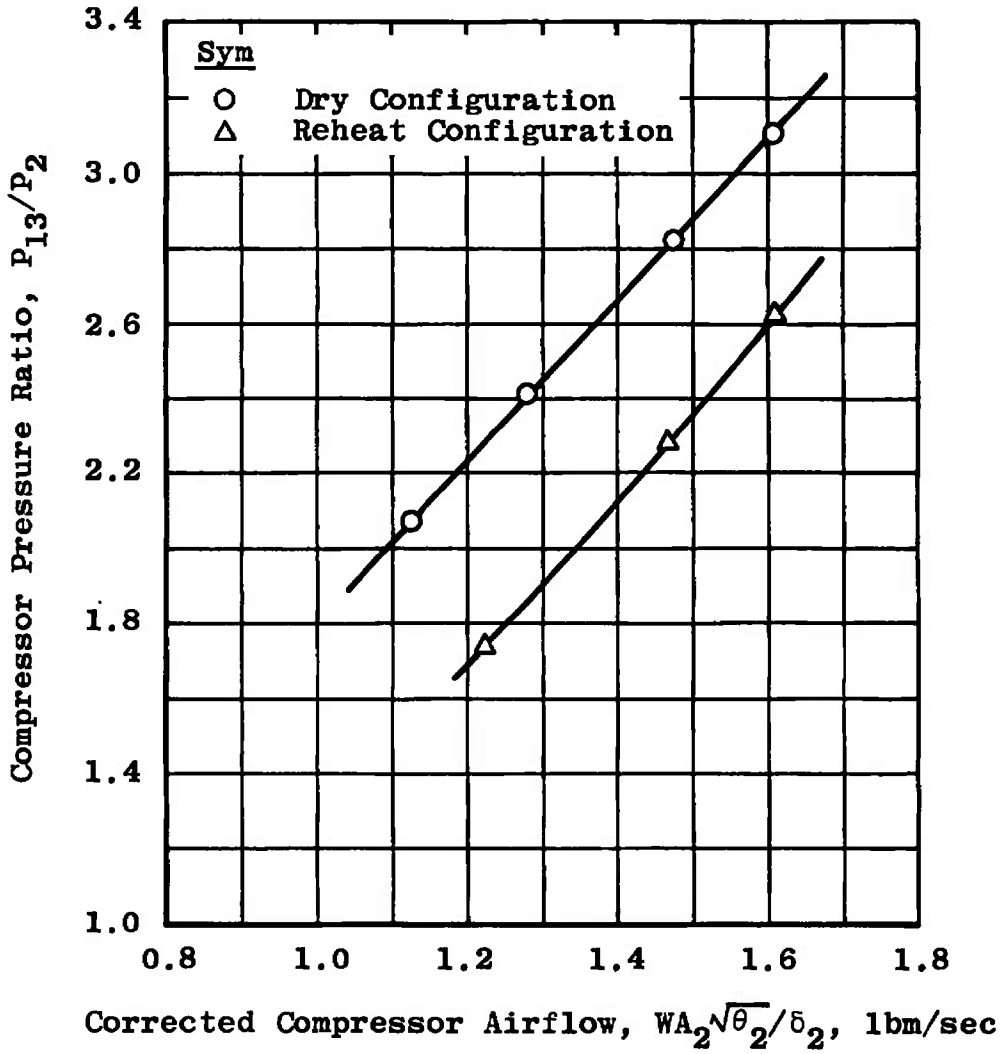
Figure 11. Nominal compressor operating lines during nozzle performance evaluation.

Simulated Flight Conditions

Sym	Mach No.	Altitude, ft
—○—	0.6	12,700
—□—	0.8	21,400
—△—	0.9	24,800
—☆—	1.2	34,200
—◇—	1.5	43,700

$T_2 = 120°F$

- - - Predicted Performance for All Flight Conditions (Ref. 4)

Predicted = 0.942
Average = 0.948

Nozzle Thrust Coefficient, $C_{F_{GI}}$

Nozzle Flow Coefficient, C_{D_8}

Nozzle Pressure Ratio, P_8/P_{AMB}
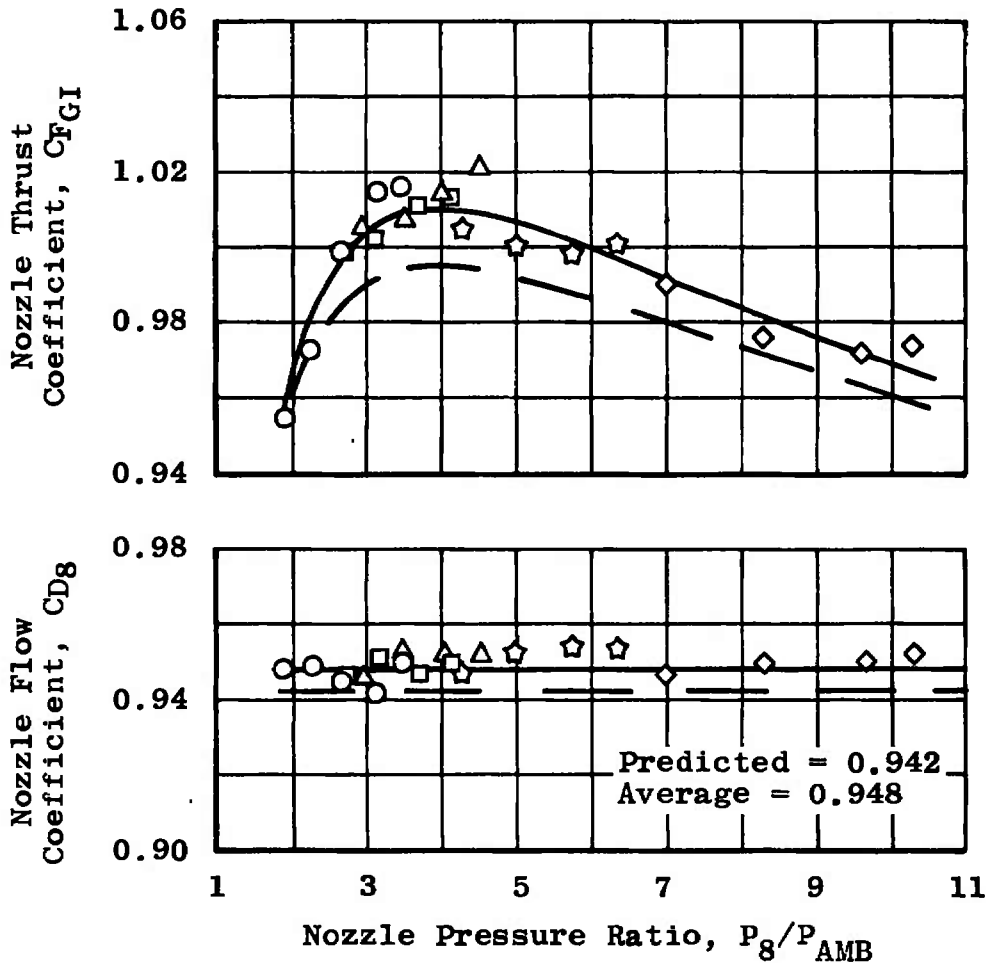
a. Dry nozzle configuration ($A_8 = 3.12$ in.²)

Figure 12. Nozzle thrust and nozzle flow coefficients as a function of nozzle pressure ratio.

47

Simulated Flight Conditions

Sym	Mach No.	Altitude, ft
—○—	0.6	12,700
—□—	0.8	21,400
—△—	0.9	24,800
—☆—	1.2	34,200
—◇—	1.5	43,700

$T_2 = 120^{\circ}F$

— — — Predicted Performance for All
Flight Conditions (Ref. 4)

b. Reheat configuration ($A_8 = 5.72$ in.^{2})
Figure 12. Concluded.

Table 1. Steady-State Measurement Uncertainty

Parameter Designation	STEADY-STATE ESTIMATED MEASUREMENT*							Range	Type of Measuring Device	Type of Recording Device	Method of System Calibration
	Precision Index (S)			Bias (B)		Uncertainty ±(B + t95S)					
	Percent of Reading	Unit of Measurement	Degree of Freedom	Percent of Reading	Unit of Measurement	Percent of Reading	Unit of Measurement				
Compressor Inlet Total Pressure, P2	±0.05	----	4	±0.15	----	±0.3	----	7 to 18 psia	Bonded Strain-Gage Type Pressure Transducers	Automatic Multiple Pressure Scanning System onto Sequential Sampling, Millivolt-to-Digital Converter, and Magnetic Tape Storage Data Acquisition	In-Place Application of Multiple Pressure Levels Measured with a Pressure-Measuring Device Calibrated in the Standards Laboratory
Compressor Exit Total Pressure, P13	±0.05	----	184	±0.12	----	±0.2	----	10 to 54 psia			
Nozzle Entrance Total Pressure, P7	±0.05	----	184	±0.12	----	±0.2	----	10 to 54 psia			
Nozzle Entrance Static Pressure, PS7	±0.05	----	4	±0.15	----	±0.3	----	7 to 48 psia			
Turbine Drive Venturi	±0.07	----	31	±0.2	----	±0.3	----	50 to 500 psia		Sequential Sampling, Millivolt-to-Digital Converter, and Magnetic Tape Storage Data Acquisition System	Resistance Shunt Based on the Standards Laboratory Determination of Transducer Applied Pressure versus Resistance Shunt Equivalent Pressure Relationship
Inlet Pressure, PV1D	±0.07	----	31	±0.2	----	±0.3	----	500 to 2700 psia			
Turbine Drive Venturi Throat Pressure, PVTD	±0.1	----	31	±0.2	----	±0.4	----	150 to 1500 psia			
Turbine Bleed Venturi	±0.07	----	31	±0.2	----	±0.3	----	15 to 100 psia			
Inlet Pressure, PV1B	±0.07	----	31	±0.2	----	±0.3	----	100 to 800 psia			
Turbine Bleed Venturi Throat Pressure, PVTB	±0.1	----	31	±0.2	----	±0.4	----	50 to 350 psia			
Compressor Venturi Inlet Pressure, PV1C	±0.07	----	31	±0.2	----	±0.3	----	15 to 40 psia			
Compressor Venturi Throat Pressure, PVTC	±0.1	----	31	±0.2	----	±0.4	----	15 to 25 psia			

*REFERENCE: Abernethy, R. B. and Thompson, J.W. Jr. "Handbook, Uncertainty in Gas Turbine Measurements." AEDC-TR-73-5 (AD755358), February 1973.

49

Table 1. Concluded

Parameter Designation	STEADY-STATE ESTIMATED MEASUREMENT[a]							Range	Type of Measuring Device	Type of Recording Device	Method of System Calibration
	Precision Index (S)			Bias (B)		Uncertainty ±(B + t95S)					
	Percent of Reading	Unit of Measurement	Degree of Freedom	Percent of Reading	Unit of Measurement	Percent of Reading	Unit of Measurement				
Test Cell Pressure, PAMB	----	+0.003 psi	31	----	+0.005 psi	----	+0.01 psi	2 to 3 psia	Bonded Strain-Gage Type Pressure Transducers	Sequential Sampling, Millivolt-to-Digital Converter, and Magnetic Tape Storage Data Acquisition System	Resistance Shunt Based on the Standards Laboratory Determination of Transducer Applied Pressure versus Resistance Shunt Equivalent Pressure Relationship
	+0.1	----		+0.15	----	+0.35	----	3 to 15 psia			
Rotor Speed, N	+0.1	----	31	+0.1	----	+0.3	----	30,000 to 85,000 rpm	Electro-mechanical Transducers	Frequency-to-Voltage Converter onto Sequential Sampling, Millivolt-to-Digital Converter, and Magnetic Tape Storage Data Acquisition System	Frequency Substitution Based on the Transducer and Transducer-to-Engine Rotor Coupling Characteristics
Scale Force, FS	----	+0.15 lbf	244	±(0.2% + 0.3 lbf)		±(0.2% + 0.6 lbf)		20 to 300 lbf	Bonded Strain-Gage-Type Force Transducers	Sequential Sampling, Millivolt-to-Digital Converter, and Magnetic Tape Storage Data Acquisition System	In-Place Application of Multiple Force Levels Measured with Force Transducers in the Standards Laboratory
Bellmouth Inlet Total Temp., T1	----	+0.6°F	191	----	+0.9°F	----	+2.°F	60 to 125°F	Chromel-Alumel Temperature Transducers	↓	Millivolt Substitution Based on the NBS Temperature versus Millivolt Tables
Compressor Exit Total Temp., T13	----	+0.6°F	191	----	+0.9°F	----	±2.°F	60 to 360°F			
				+0.25	----	±(0.25% + 1.2°F)	----	360 to 450°F			
Nozzle Entrance Total Temperature, T7	----	+0.6°F	191	----	+0.9°F	----	+2.°F	60 to 360°F			
				+0.25	----	±(0.25% + 1.2°F)	----	360 to 450°F			
Turbine Inlet Total Temp., T4	----	+0.6°F	191	----	+0.9°F	----	+2.°F	60 to 360°F			
				+0.25	----	±(0.25% + 1.2°F)	----	360 to 450°F			
Turbine Exit Total Temp., T5	----	+0.6°F	191	----	+0.9°F	----	+2.F	20 to 150°F	↓	↓	↓

APPENDIX A
METHODS OF CALCULATION

The general method and equations used to compute the parameters presented in this report are presented in this Appendix. Where applicable, the arithmetic average of the pressures and temperatures were used.

SPECIFIC HEATS

The ratio of specific heats was obtained by

$$\gamma = \frac{C_p}{C_p - \frac{R}{778}}$$

where

$$R = 53.342$$

and the specific heat at constant pressure was calculated using

$$C_p = 0.2318 + (1.04 \times 10^{-5}) T + (7.166 \times 10^{-9}) T^2$$

TOTAL TEMPERATURE

Total temperature measurements made inside the simulator were corrected for probe design in the following manner:

$$T = \frac{T_{indicated}}{correction\ factor}$$

Correction factors were provided by the General Electric Company.

MACH NUMBER

For stations 0, 1, 13, 5, 8, and 9 where both the static and total pressure were measured, the Mach number was obtained from the equation:

$$M_p = \left\{ \frac{2}{\gamma - 1} \left[\left(\frac{P}{PS} \right)^{\frac{\gamma-1}{\gamma}} - 1 \right] \right\}^{\frac{1}{2}}$$

An iterative procedure based on continuity was used to calculate Mach number at stations 15, 17, 58, and 7.

$$M_w = f(W, A, T, P)$$

AIRFLOWS

Compressor Inlet Airflow

The compressor inlet airflow was measured with a critical flow venturi and calculated as follows:

For critical flow,

$$WA_{IN} = C_t\, C_f\, P_{VI}\, A_{VT} \sqrt{\frac{\gamma G}{RT}} \left(\frac{2}{\gamma + 1} \right)^{\frac{(\gamma+1)}{2(\gamma-1)}}$$

For subcritical flow,

$$WA_{IN} = C_t\, C_f\, P_{VI}\, A_{VT} \left\{ \frac{2G}{RT} \left(\frac{\gamma}{\gamma - 1} \right) \left(\frac{P_{VI}}{P_{VT}} \right)^{\frac{\gamma-1}{\gamma}} \left[\left(\frac{P_{VI}}{P_{VT}} \right)^{\frac{\gamma-1}{\gamma}} - 1 \right] \right\}^{\frac{1}{2}}$$

where C_t is the area thermal expansion coefficient from the venturi throat adiabatic wall temperature, and C_f is an experimentally determined flow coefficient. C_t and C_f are discussed in detail in Appendix B.

Turbine Drive and Turbine Bleed Airflows

The turbine drive (W_{DM}) and turbine bleed (W_{BM}) airflows were measured with critical flow venturis and calculated as follows:

For critical flow,

$$W = C^*\, C_t\, C_f\, P_{VI}\, A_{VT} \sqrt{\frac{G}{RT}}$$

For subcritical flow,

$$W = \frac{C^*}{C^*_{ideal}} C_t C_f P_{VT} A_{VT} \left\{ \frac{2G}{RT} \left(\frac{\gamma}{\gamma-1} \right) \left(\frac{P_{VI}}{P_{VT}} \right)^{\frac{\gamma-1}{\gamma}} \left[\left(\frac{P_{VI}}{P_{VT}} \right)^{\frac{\gamma-1}{\gamma}} - 1 \right] \right\}^{\frac{1}{2}}$$

where C_t is the area thermal expansion coefficient from the venturi throat adiabatic wall temperature, C_f is an experimentally determined flow coefficient, and C^* is the real gas coefficient. C_t, C_f, and C^* are discussed in detail in Appendix B.

Airflows at other stations were obtained in the following manner:

Simulator Inlet Airflow $\qquad W_1 = WA_{IN}$

Compressor Inlet Airflow $\qquad W_2 = W_1$

Compressor Exit Airflow $\qquad W_{13} = W_2$

Bearing Cooling Airflow $\qquad W_{c_4} = 0.0075 \, W_4$

Duct Inlet Airflow $\qquad W_{15} = W_{13} + W_{c_4}$

Duct Airflow at Mixer Entrance $\qquad W_{17} = W_{15}$

Turbine Inlet Airflow $\qquad W_4 = W_{DM}/1.0075$

Thrust Trim Orifice Airflow $\qquad WIN_6 = \dfrac{0.53177 \, (PS_{108}) \, A_{TTO} \, C_{d_{TTO}}}{\sqrt{T_5}}$

where

$$A_{TTO} = 0.02688$$

and

$$C_{d_{TTO}} = \left. \begin{array}{l} 0.0 \text{ for } PS_{108}/PS_{58} < 1.0 \\ 1.0 \text{ for } PS_{108}/PS_{58} = 1.0 \\ 4.0 \text{ for } PS_{108}/PS_{58} \geq 4.0 \end{array} \right\} \text{ straight line segments}$$

Mixer Exit Airflow $\qquad W_{58} = W_{13} - W_{DM} - W_{BM}$

Nozzle Entrance Airflow $\qquad W_7 = W_{58}$

Nozzle Throat Airflow $\qquad W_8 = W_7$

CORRECTED AIRFLOW AND ROTOR SPEED

The compressor inlet airflow and compressor rotor speed were corrected to standard sea-level conditions by the following relationships:

$$WA_{2R} = W_2 \sqrt{\theta_2}/\delta_2 \qquad \text{and} \qquad N_{R_2} = N/\sqrt{\theta_2}$$

where

$$\theta_2 = \frac{T_2(^\circ R)}{518.7} \qquad \text{and} \qquad \delta_2 = P_2/14.696$$

NOZZLE THROAT TOTAL PRESSURE

The nozzle throat total pressure was calculated from the following equation:

$$P_8 = P_7 - 0.0036\, \gamma\, PS_{7\,w}(M_{7\,w})^2$$

ISENTROPIC NOZZLE EXIT AIRFLOW

Isentropic nozzle exit airflow was calculated as follows:

For choked flow,

$$W_{8_I} = P_8 A_8 \sqrt{\left(\frac{2}{\gamma+1}\right)^{\frac{\gamma-1}{\gamma-1}} \frac{\gamma G}{R T_7}}$$

For unchoked flow,

$$W_{8_I} = A_8 \frac{P_{AMB}}{R T_7} \left(\frac{P_8}{P_{AMB}}\right)^{\frac{\gamma-1}{\gamma}} \sqrt{\left(\frac{2G\,\gamma\,T_7}{\gamma-1}\right)\left[1 - \left(\frac{P_{AMB}}{P_8}\right)^{\frac{\gamma-1}{\gamma}}\right]}$$

NOZZLE FLOW COEFFICIENT

The nozzle flow coefficient was calculated from the equation:

$$C_{d_8} = \frac{W_8}{W_{8_I}} = \frac{A_{8_{effective}}}{A_8}$$

where

$$A_{8_{effective}} = \frac{W_8 \sqrt{T_7}}{P_8 \left(\frac{2}{\gamma + 1}\right)^{\frac{\gamma+1}{2(\gamma-1)}} \sqrt{\frac{\gamma G}{R}}}$$

THRUST

Scale Force

For a discussion of scale force, see Appendix C.

Gross Thrust

Gross thrust was calculated from the following equations:

$$FG = FS + \frac{W_1 V_1}{G} + (PS_1 - P_{AMB}) A_{seal}$$

where

$$V_1 = M_1 \sqrt{\frac{\gamma G R T_1}{1 + \frac{\gamma - 1}{2} M_1^2}}$$

Isentropic Gross Thrust

Isentropic gross thrust was calculated from the following equation:

$$FG_I = W_8 \sqrt{\frac{R T_8}{G} \frac{2\gamma}{\gamma - 1} \left[1 - \left(\frac{P_{AMB}}{P_8}\right)^{\frac{\gamma-1}{\gamma}}\right]}$$

Nozzle Thrust Coefficient

The nozzle thrust coefficient was calculated from the following equation:

$$C_{f_{GI}} = \frac{FG}{FG_I}$$

NOZZLE PRESSURE AND TEMPERATURE DISTORTION

$$Distortion = \frac{Maximum - Minimum}{Average} \times 100 \text{ percent}$$

APPENDIX B
VENTURI MASS FLOW CALCULATIONS

Three venturis were used to meter airflow rates at the compressor inlet (compressor venturi), the turbine drive system inlet (drive venturi), and the turbine drive system exit (bleed venturi). The method for calculating the air mass flow rates through the venturis is presented in this Appendix.

GENERAL VENTURI EQUATIONS

The air mass flow rates through the venturis were calculated using the following equations:

Venturi Mass Flow Rate Equations

For choked flow through the compressor venturi, the flow rate is given by

$$W = C_t C_f PS_{VI} A_{VT} \sqrt{\frac{\gamma G}{RT}} \left(\frac{2}{\gamma - 1}\right)^{\frac{\gamma+1}{2(\gamma-1)}} \tag{B-1}$$

For choked flow through the turbine drive system venturis, the flow rates are given by

$$W = C^* C_t C_f PS_{VI} A_{VT} \sqrt{G/RT} \tag{B-2}$$

Supporting Equations

The venturi throat diameter (D_{VT}), the inlet static pressure (PS_{VI}), the throat static pressure (PS_{VT}), and the total temperature (T) were measured parameters. The throat area was calculated by

$$A_{VT} = (\pi/4) D_{VT}^2 \tag{B-3}$$

where

$$D_{VT} = 1.6584 \text{ in. (compressor venturi)}$$
$$= 0.8903 \text{ in. (bleed venturi)}$$
$$= 0.3733 \text{ in. (drive venturi)}$$

The coefficient for effects of thermal growth is given by

$$C_t = [1 - \alpha (T - T_{ref})]^2 \tag{B-4}$$

In Eq. (B-1), the ratio of specific heats (γ) was obtained by

$$\gamma = \frac{C_p}{C_p - \frac{R}{778}}$$ (B-5)

where the specific heat at constant pressure was calculated using

$$C_p = 0.2318 - (1.04 \times 10^{-5}) T + (7.166 \times 10^{-9})T^2$$ (B-6)

The methods employed to obtain the configuration (flow) coefficients (C_f) and the critical flow factors (C^*) are presented in the following sections.

Configuration Coefficients

The three venturis were calibrated by the Colorado Engineering Experiment Station, Inc., (CEESI). In each case, the venturi, with its associated instrumentation (thermocouples and pressure transducers), was calibrated against a standard CEESI critical flow venturi (secondary standard) which had been, in turn, calibrated against weigh tanks.

CEESI measured flow rate, inlet static pressure, and total temperature, from which a "discharge coefficient" was obtained. By using the values for inlet static pressure and total temperature provided by CEESI, a "Reynolds Number Parameter" was calculated by

$$R_{NP} = \frac{PS_{VI} \; D_{VT}}{\mu} \sqrt{\frac{\gamma}{GRT}}$$ (B-7)

where

$$\gamma = 1.4$$

and

$$\mu = (2.27 \times 10^{-8})\left(\frac{T^{*(3/2)}}{T^* + 198.6}\right)$$ (B-8)

with the throat static temperature given by

$$T^* = T \left(\frac{TS}{T}\right)_{throat}$$ (B-9)

The temperature ratio used in Eq. (B-9) is the following:

$$\left(\frac{TS}{T}\right)_{throat} = 0.8333 \qquad (B-10)$$

for the compressor venturi, and

$$\left(\frac{TS}{T}\right)_{throat} = 0.833613 - 1.14635 \times 10^{-4} \, PS_{VI} + 9.5706 \times 10^{-8} \, PS_{VI}^2 \qquad (B-11)$$

for the turbine drive venturi, and

$$\left(\frac{TS}{T}\right)_{throat} = 0.832972 - (1.53003 \times 10^{-4}) PS_{VI} + 1.81833 \times 10^{-7} \, PS_{VI}^2 \qquad (B-12)$$

for the bleed venturi. Equations (B-11) and (B-12) are based on data from Refs. 7 and 8, and the pressure (PS_{VI}) used in the equations is in atmospheres.

Note that the Reynolds number parameter of Eq. (B-7) is related to the conventional Reynolds number by

$$R_{NP} = R_N \left(\frac{PS_{VI}}{P^*}\right) \left(\frac{T}{T^*}\right)^{1/2} \qquad (B-13)$$

For choked flow of ideal gas, the pressure and temperature ratios are constants.

The CEESI "discharge coefficient" data for the three venturis are presented in Fig. B-1 as a function of the Reynolds number parameter. The calibrations were conducted over the following ranges of inlet static pressure and total temperature:

Venturi	PS_{VI} Range, psia	T Range, °R
Compressor	5.0 to 40.1	548 to 565
Turbine Bleed	33.0 to 250.5	553 to 579
Turbine Drive	212.0 to 2,824	518 to 612

The CEESI data were not corrected for the difference between the measured inlet static pressure (PS_{VI}) and the true total pressure (P_{VI}). This resulted in some of the coefficients exceeding unity. However, since the measured PS_{VI} was used both in the calibration data and the test data, the correction was not necessary.

The CEESI data were corrected for thermal growth (C_t) to a common base of T_{ref} = 540°R. This resulted in the "configuration coefficient" (C_f) that is presented in Fig. B-2 as a function of the Reynolds number parameter. Equations of the form

$$C_f = A_o + A_1 (\log_{10} R_{NP}) + A_2 (\log_{10} R_{NP})^2 + A_3 (\log_{10} R_{NP})^3 \qquad (B-14)$$

were obtained to approximate the data of Fig. B-2. Values of A_o, A_1, A_2, and A_3 for each of the three venturis are presented in Table B-1, and the curves defined by Eq. (B-14) are shown in Fig. B-2.

To show the effect of the inlet static pressure to total pressure correction, the data from Fig. B-2 is presented in Fig. B-3 with the correction incorporated.

Critical Flow Factor

The critical flow factor (C^*) used in Eqs. (B-1) and (B-2) is defined in Ref. 7 as

$$C^* = \frac{W}{A_{VT} P_{VI}} \sqrt{\frac{RT}{G}} \qquad (B-15)$$

for ideal air ($\gamma = 1.4$),

$$C^*_{ideal} = \left[\gamma \left(\frac{2}{\gamma + 1} \right)^{\frac{\gamma+1}{2(\gamma-1)}} \right] = 0.68473146 \qquad (B-16)$$

Johnson presented analytical values of C^* for air (real gas) at total pressures of up to 100 atm and total temperatures between 400 and 700°R in Ref. 7. Johnson also published analytical values of C^* for nitrogen at total pressures of up to 300 atm in Ref. 8. The Colorado Engineering Experimental Station, Inc., extrapolated the air data (Ref. 7) to 300 atm total pressure based on the nitrogen data (Ref. 8). CEESI then obtained equations for C^* of the form

$$C^* = X_o + X_1 P_{VI} + X_2 P_{VI}^2 + X_3 P_{VI}^3 + X_4 P_{VI}^4 + X_5 P_{VI}^5 + X_6 P_{VI}^6 \qquad (B-17)$$

where P_{VI} is in atmospheres. The values of the coefficients (X_o,...,X_6) for each total temperature are presented in Table B-2. The values of C^* generated by the CEESI equations are shown in Fig. B-4.

In order to collapse the CEESI family of equations for C^* to a general equation to be used over the range of pressure and temperature of interest (i.e. $0 \leqslant P_{VI} \leqslant 200$ atm and $500 \leqslant T \leqslant 700°R$), the CEESI equation for C^* at $T = 500°R$ (C^*_{500}) was taken as a base line. A correction for temperature was applied to C^*_{500}, with the correction being both temperature and pressure dependent. An equation was assumed of the form:

$$C^* = C^*_{500} - \Delta C^* (P_{VI}) f(T) \qquad (B-18)$$

The base line value of C^* (at $T = 500°R$) is

$$C^*_{500} = B_o + B_1 P_{VI} + B_2 P^2_{VI} + B_3 P^3_{VI} + B_4 P^4_{VI} + B_5 P^5_{VI} + B_6 P^6_{VI} \qquad \text{(B-19)}$$

where P_{VI} is in atmospheres, and

$$B_o = 0.685106 \qquad \text{(B-20a)}$$

$$B_1 = 3.03978 \times 10^{-4} \qquad \text{(B-20b)}$$

$$B_2 = 1.82024 \times 10^{-6} \qquad \text{(B-20c)}$$

$$B_3 = -2.16299 \times 10^{-8} \qquad \text{(B-20d)}$$

$$B_4 = 8.78701 \times 10^{-11} \qquad \text{(B-20e)}$$

$$B_5 = -1.70062 \times 10^{-13} \qquad \text{(B-20f)}$$

$$B_6 = 1.25600 \times 10^{-16} \qquad \text{(B-20g)}$$

The term $\Delta C^*(P_{VI})$ is the maximum correction (i.e. from $T = 500°R$ to $T = 700°R$ and is a function of P_{VI} only (Fig. B-5). That is,

$$\Delta C^*(P_{VI}) = C^*_{500} - C^*_{700} \qquad \text{(B-21)}$$

This term can be expressed as

$$\Delta C^*(P_{VI}) = C_o + C_1 P_{VI} + C_2 P^2_{VI} + C_3 P^3_{VI} + C_4 P^4_{VI} + C_5 P^5_{VI} \qquad \text{(B-22)}$$

where P_{VI} is in atmospheres, and

$$C_o = 6.65868 \times 10^{-4} \qquad \text{(B-23a)}$$

$$C_1 = 2.23355 \times 10^{-4} \qquad \text{(B-23b)}$$

$$C_2 = 1.34744 \times 10^{-6} \qquad \text{(B-23c)}$$

$$C_3 = -1.29795 \times 10^{-8} \qquad \text{(B-23d)}$$

$$C_4 = 4.11025 \times 10^{-11} \qquad \text{(B-23e)}$$

$$C_5 = -4.94097 \times 10^{-14} \qquad \text{(B-23f)}$$

The term $f(T)$, used to adjust the correction for values of T other than $700°R$, varies from 0.0 at $T = 500°R$ to 1.0 at $T = 700°R$ and is of the form

$$f(T) = \frac{C^*_{500} - C^*_T}{C^*_{500} - C^*_{700}} = \frac{C^*_{500} - C^*_T}{\Delta C^*(P_{VI})} \qquad \text{(B-24)}$$

The above function of T is shown in Fig. B-6 for $P_{VI} = 130$ atm. It was found that the curve (Fig. B-6) is approximately the same for all values of P_{VI} and is given by

$$f(T) = D_o + D_1 (\Delta T) + D_2 (\Delta T)^2 + D_3 (\Delta T)^3 \qquad \text{(B-25)}$$

where

$$\Delta T = T - 500°R \qquad \text{(B-26)}$$

$$D_o = 3.81429 \times 10^{-4} \qquad \text{(B-27a)}$$

$$D_1 = 9.69248 \times 10^{-3} \qquad \text{(B-27b)}$$

$$D_2 = -3.49957 \times 10^{-5} \qquad \text{(B-27c)}$$

$$D_3 = 5.76667 \times 10^{-8} \qquad \text{(B-27d)}$$

In the application of Eqs. (B-18), (B-19), (B-22), and (B-25), the measured inlet static pressure (PS_{VI}) was used in place of the total pressure (P_{VI}). This resulted in an error of less than 0.04 percent in the calculated values of C*.

TURBINE DRIVE SYSTEM VENTURIS

The turbine drive system venturis (drive and bleed) were checked against each other by connecting the two venturis in series such that all air flowing through one also flowed through the other. The flow rates through each venturi were calculated, and the results were compared. The ratio of the calculated mass flow rates (W_{BM}/W_{DM}) is presented in Fig. B-5 as a function of the drive venturi flow rate (W_{DM}). Ideally, the ratio should have been 1.00 for all conditions.

The reasons for the discrepancy between the calculated flow rates for the two venturis (Fig. B-6) are not known because a thorough investigation was beyond the scope of the test program. However, it is suspected that the' primary source of error may be found in the calculation of the real gas effects coefficients (C*). Therefore, the bleed venturi flow rate calculations would be more accurate than the drive venturi flow rate calculations because the air flowing through the bleed venturi was closer to ideal than that flowing through the drive venturi.

In order to force agreement between the flow rates of the drive and bleed venturis, a "correction factor" was applied to the drive venturi flow rate. The solid line curve shown in Fig. B-6 was taken as the correction factor and is of the form

$$C_{W_{DM}} = Y_o + Y_1 (W_{DM}) + Y_2 (W_{DM})^2 \qquad \text{(B-28)}$$

where

$$Y_0 = 1.00012 \qquad\qquad \text{(B-29a)}$$

$$Y_1 = -0.00322819 \qquad\qquad \text{(B-29b)}$$

$$Y_2 = 0.0001982 \qquad\qquad \text{(B-29c)}$$

then

$$W_{DM_{corrected}} = (W_{DM})(C_{W_{DM}}) \qquad\qquad \text{(B-30)}$$
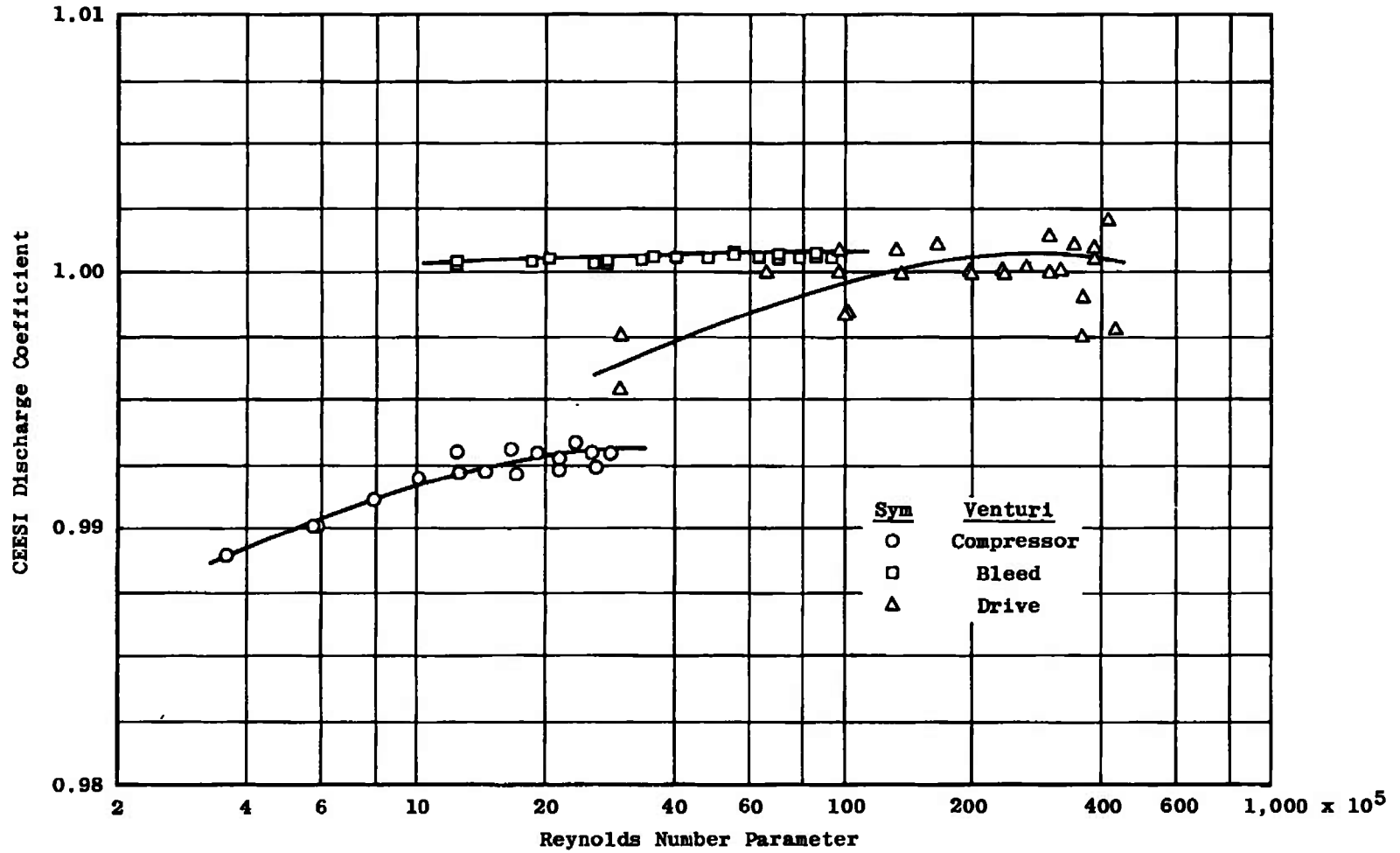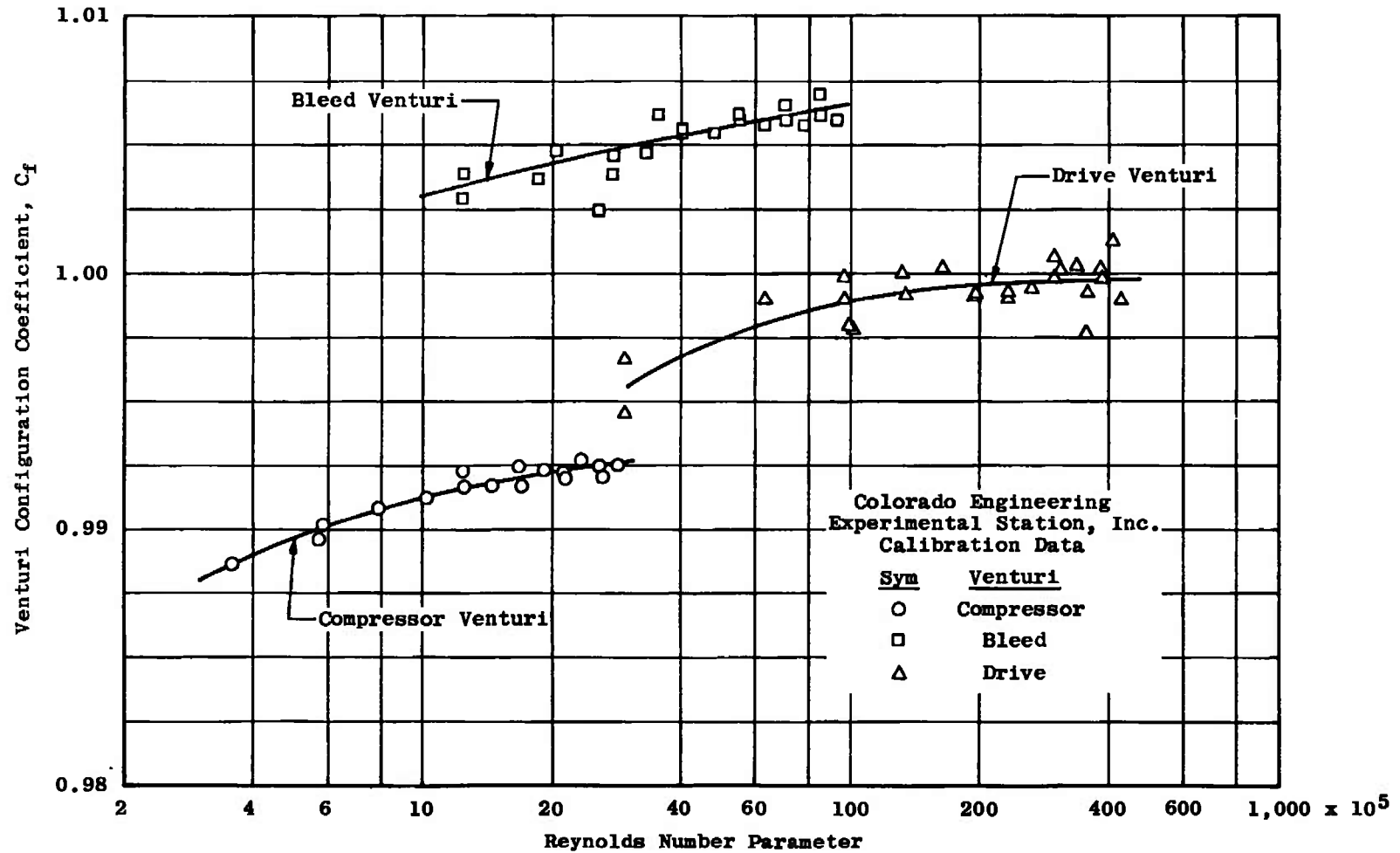
Figure B-1. CEESI venturi calibration results.

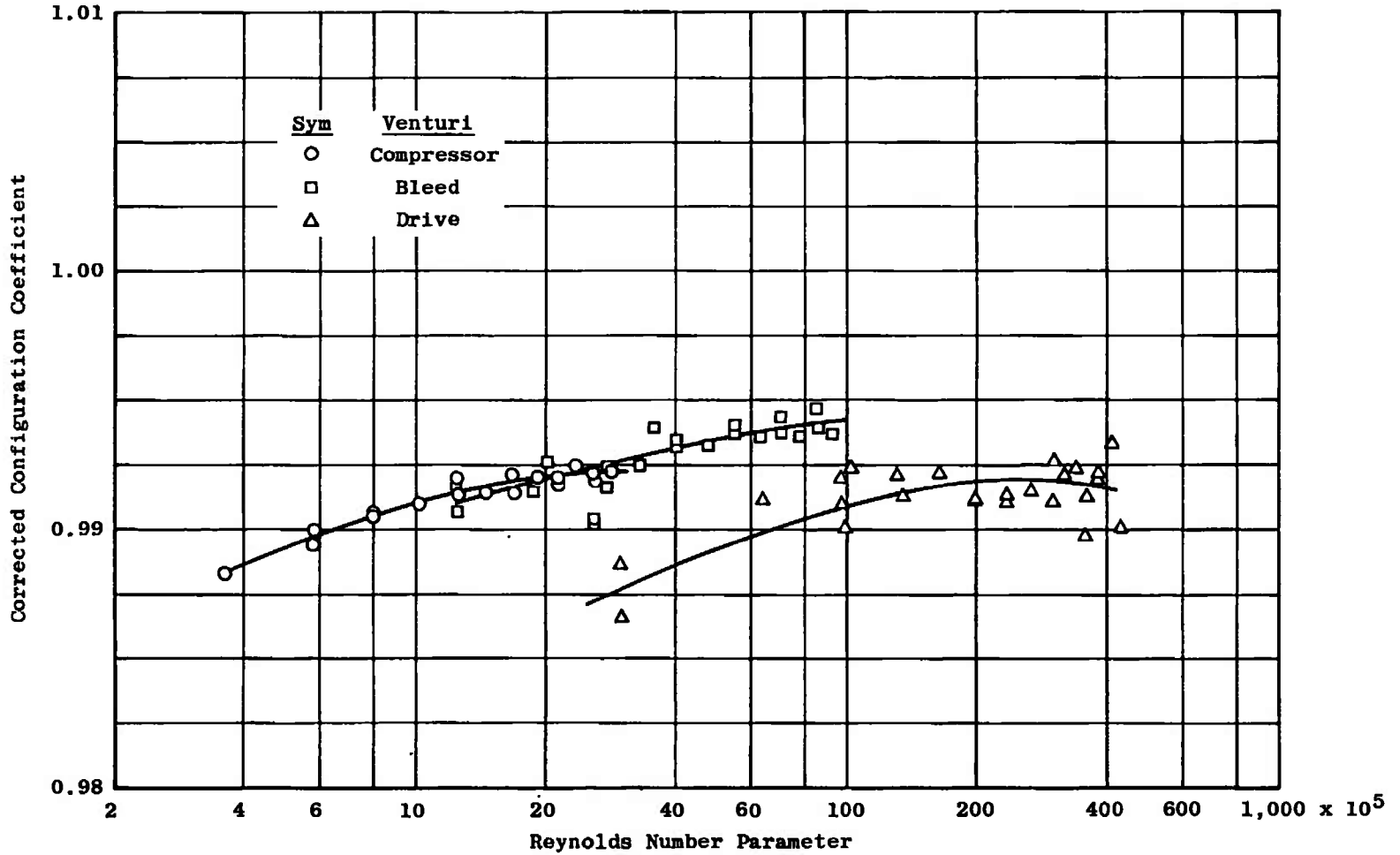Figure B-2. Venturi configuration coefficients.

Figure B-3. Venturi configuration coefficients corrected to total pressure.
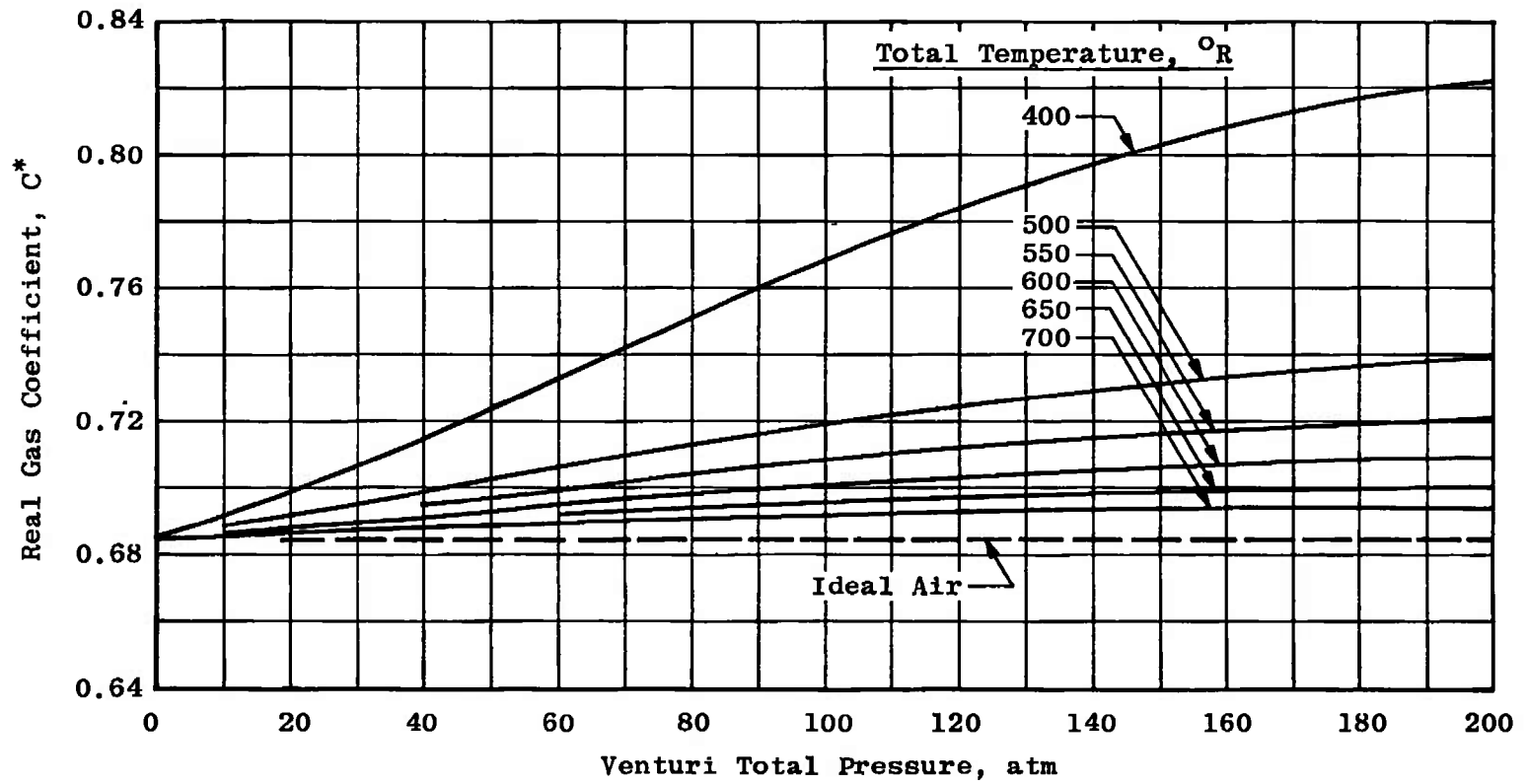
Figure B-4. Critical flow factor for air (Colorado Engineering Experimental Station, Inc., equations).
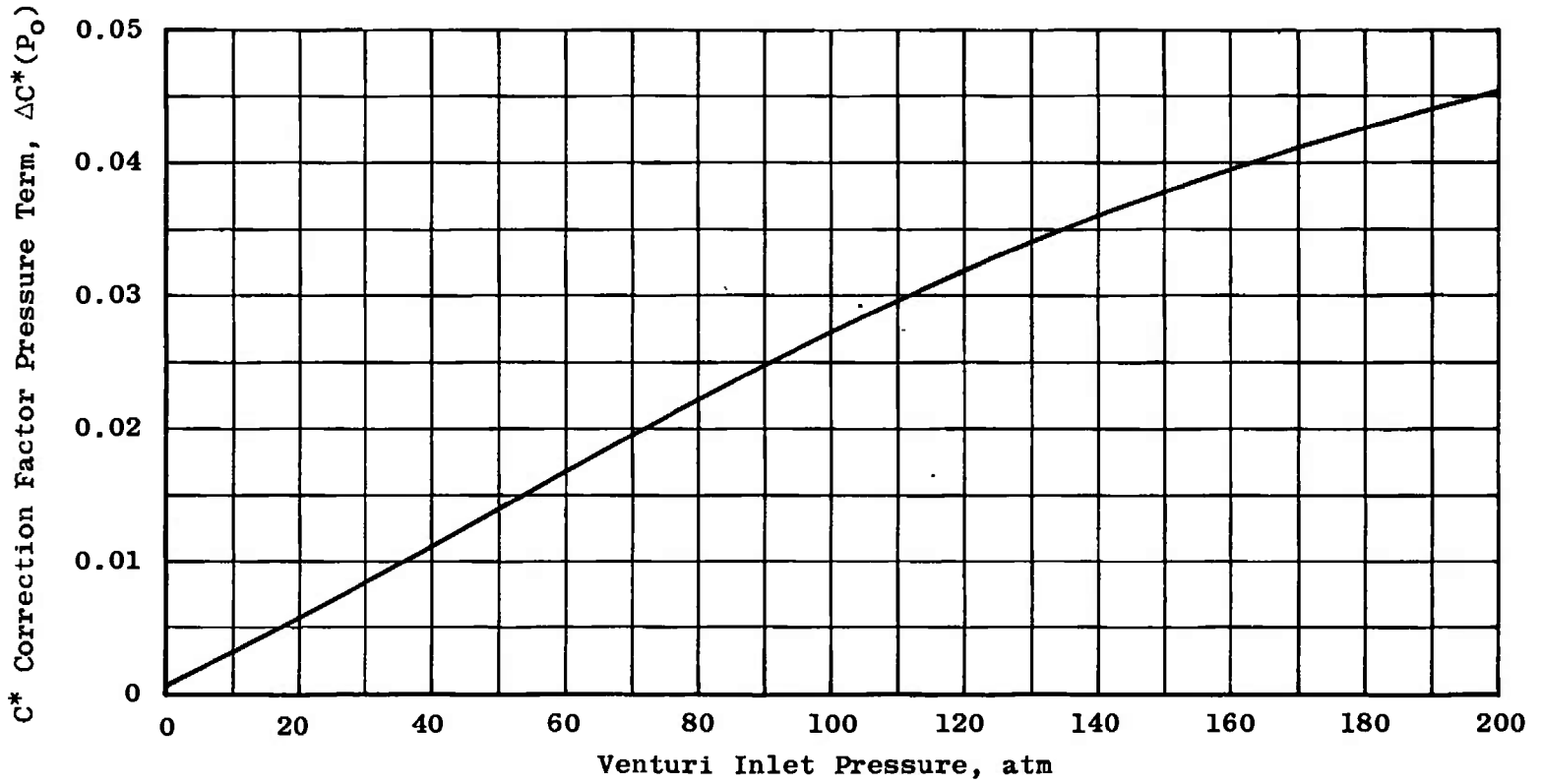
Figure B-5. Pressure dependent term to correction factor for critical flow factor equation.
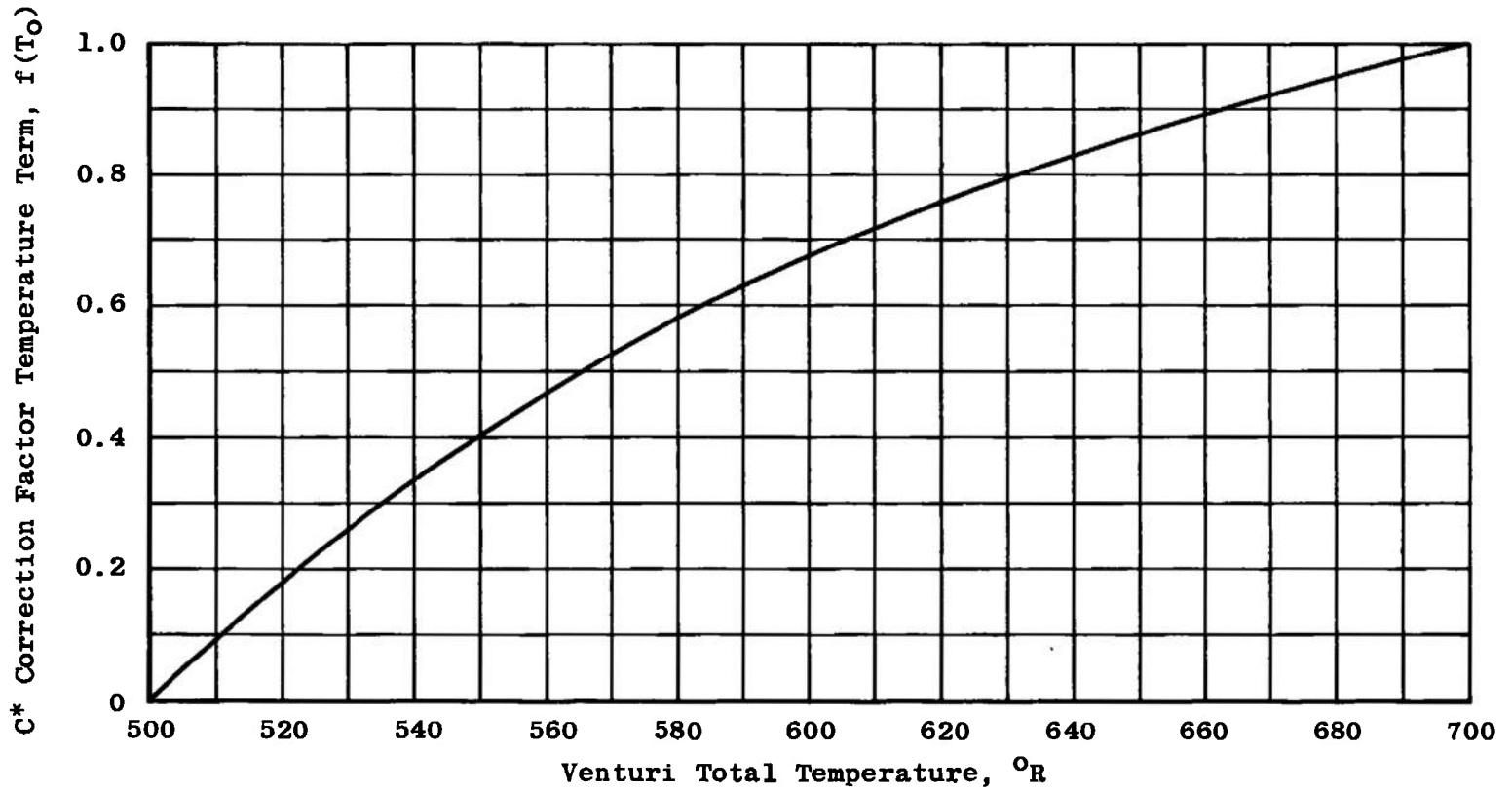
Figure B-6. Temperature dependent term to correction factor for critical flow factor equation.
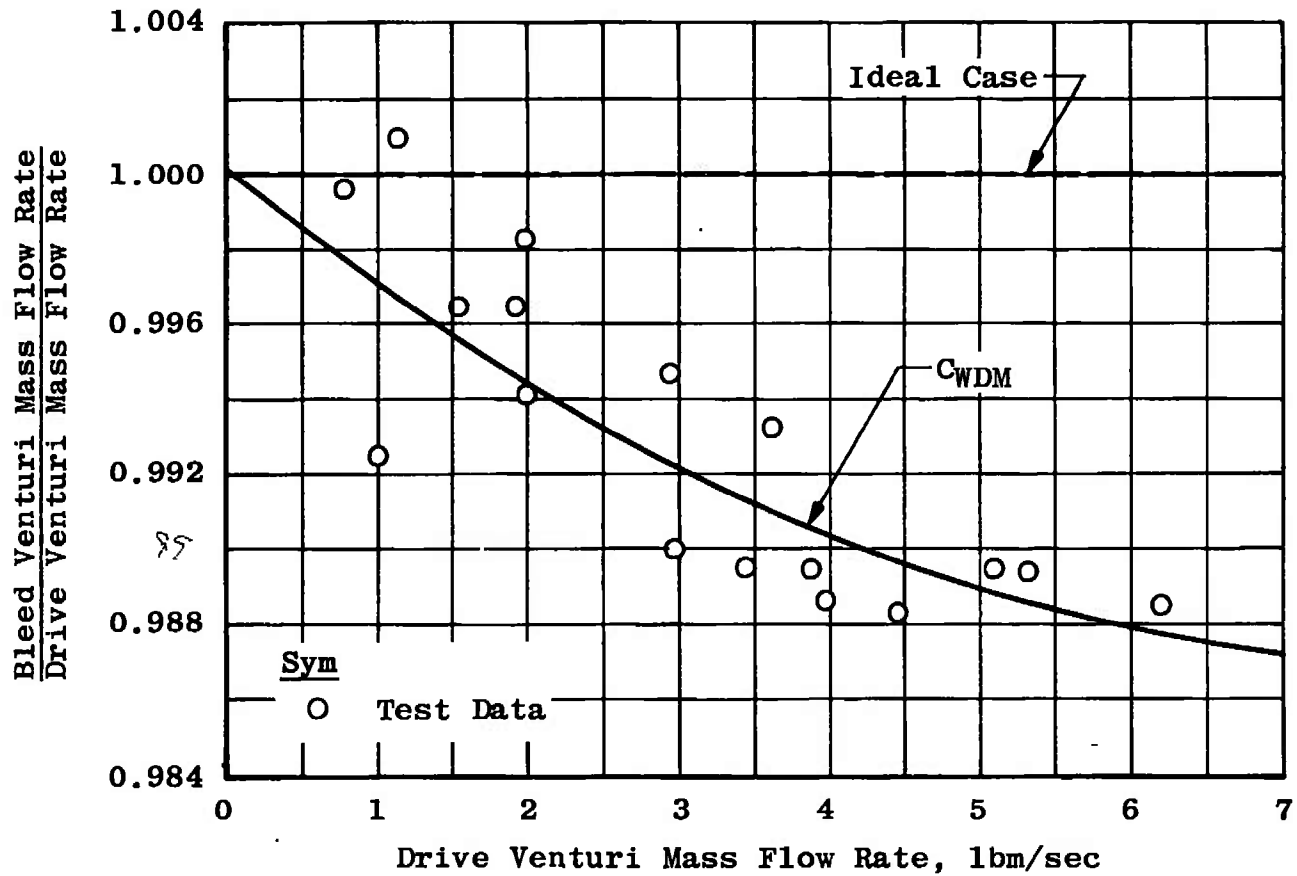
Figure B-7. Comparison of mass flow rates through turbine drive system venturis.

Table B-1. Coefficients for C_f Equations

Venturi	A_0	A_1	A_2	A_3
Compressor	0.846479	0.0438225	-0.00328331	0.0
Drive	-0.16308	0.458474	-0.0603118	0.00264716
Bleed	1.13187	-0.0730178	0.01289	-0.000716623

Table B-2. Coefficients for Colorado Engineering Experimental Station, Inc., Equation for C*

T_0, °R	X_0	$X_1 \times 10^4$	$X_2 \times 10^6$	$X_3 \times 10^8$	$X_4 \times 10^{11}$	$X_5 \times 10^{13}$	$X_6 \times 10^{16}$
400	0.685527	5.65776	6.01840	-3.85768	3.04975	2.19090	-4.15515
420	0.685362	5.01266	4.70086	-3.81525	9.62344	-0.66450	-0.54085
440	0.685255	4.47263	3.48529	-3.15870	9.52251	-1.17165	0.28137
460	0.685194	3.89589	2.93631	-3.05066	11.4586	-2.08345	1.46052
480	0.685141	3.42525	2.38259	-2.68980	10.9162	-2.16070	1.67582
500	0.685106	3.03978	1.82024	-2.16299	8.78701	-1.70062	1.25600
550	0.684923	2.22531	1.12523	-1.56421	6.96597	-1.47787	1.21197
600	0.684789	1.61024	0.76877	-1.18759	5.46512	-1.15126	0.90407
650	0.684695	1.12056	0.61799	-0.99872	4.85769	-1.09454	0.94243
700	0.684439	0.81065	0.44758	-0.81203	4.16922	-0.98159	0.88125

$$C^* = X_0 + X_1\, P_{VI} + X_2\, P_{VI}^2 + X_3\, P_{VI}^3 + X_4\, P_{VI}^4 + X_5\, P_{VI}^5 + X_6\, P_{VI}^6$$

APPENDIX C
SCALE FORCE CALCULATIONS

Scale force was calculated from the following equation:

$$FS = FS_{measured} + \Delta FS_T + \Delta FS_p + \Delta FS_S$$

The scale force equation included the following four corrections:

1. Ambient pressure and temperature calibration data load cell mechanical tare correction.

2. Inlet air seal differential pressure tare correction (ΔFS_S)

3. Temperature tare correction (ΔFS_T)

4. Load cell pressure correction (ΔFS_P)

AMBIENT CALIBRATION TARE CORRECTIONS

The thrust measuring system and inlet air seal tare corrections were determined by an in-place calibration. Force levels, measured with force transducers (load cells) calibrated in the Standards Laboratory, were applied to the thrust stand, and the resultant scale force was measured. The system tare, the difference between the scale force measurement and the applied forces, is presented in Fig. C-1. Three step resistance shunt equivalent forces were obtained from Fig. C-1 to account for the system tare force.

The system tare check was repeated after the reheat mixer failure (see Section 4.4), and three step resistance shunt equivalent forces were obtained. The difference of nominally 1 lbf in the two sets of equivalent forces was due to an undefined shift in the thrust measuring system. An average of the two ambient calibrations of equivalent forces was used for all tests prior to the mixer failure. The post mixer failure equivalent forces were used for all tests after the mixer failure.

INLET AIR SEAL TARE CORRECTION

The system tare check was performed with various differential pressures across the inlet air seal. The results, are shown in Fig. C-2. The inlet air seal tare is the variation in the system tare with inlet air seal differential pressure. The inlet air seal correction, obtained from Fig. C-2, was

$$\Delta FS_S = 0.0127777 \, (PS_1 - P_{AMB})^2 + 0.228333 \, (PS_1 - P_{AMB})$$

for $PS_1 > P_{AMB}$

and

$$\Delta FS_S = 0.0$$

for $PS_1 \leqslant P_{AMB}$

TEMPERATURE TARE CORRECTION

The procedure used to determine the temperature tare was to operate the simulator at idle rotor speed and near sea-level-static conditions. Upon reaching steady-state temperature conditions, the emergency shutdown system was activated. Shutdowns were accomplished at turbine inlet temperatures (T_4) of 150, 200, and 230°F in all combinations of compressor inlet temperatures (T_2) of 100, 110, 120, and 125°F. The temperature tare, the variation of scale force with turbine and compressor inlet temperatures, is presented in Fig. C-3. The temperature tare correction, obtained from Fig. C-3, was:

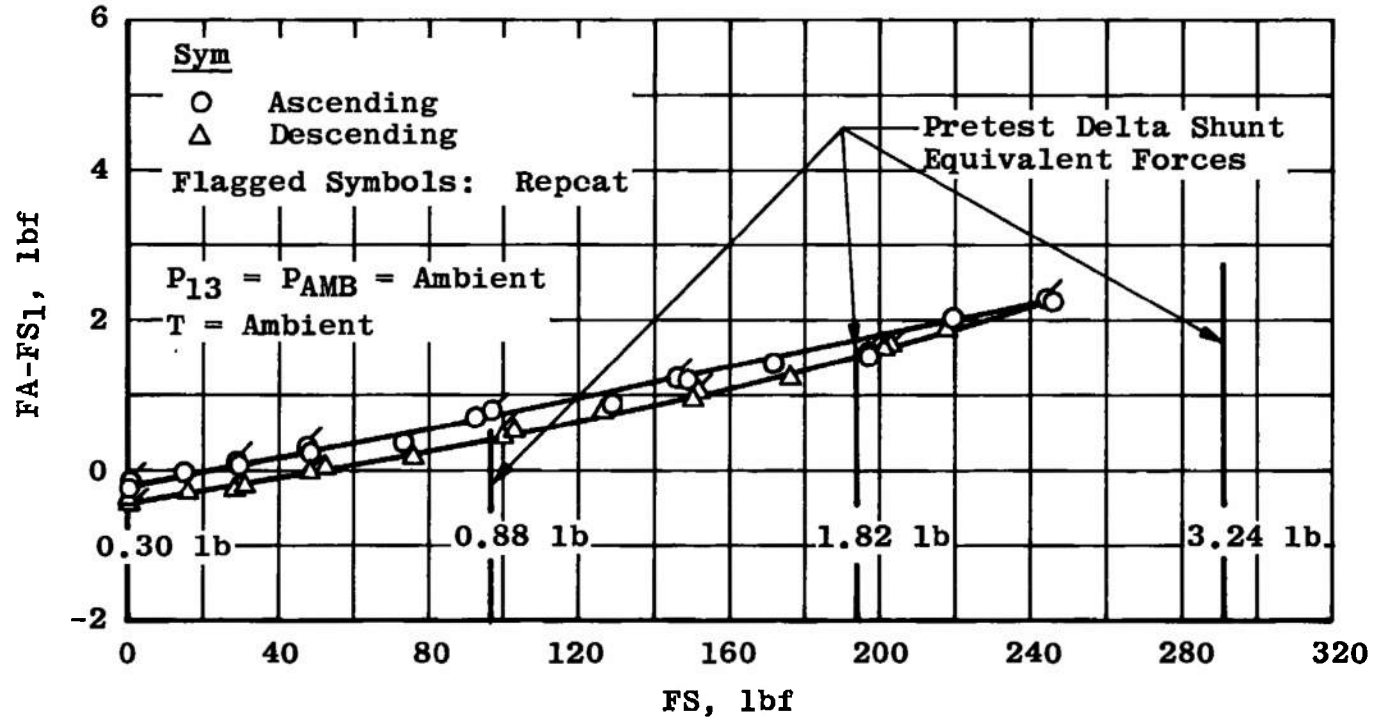$$\Delta FS_T = 0.0212222 \, T_4 - 2.343333$$

where

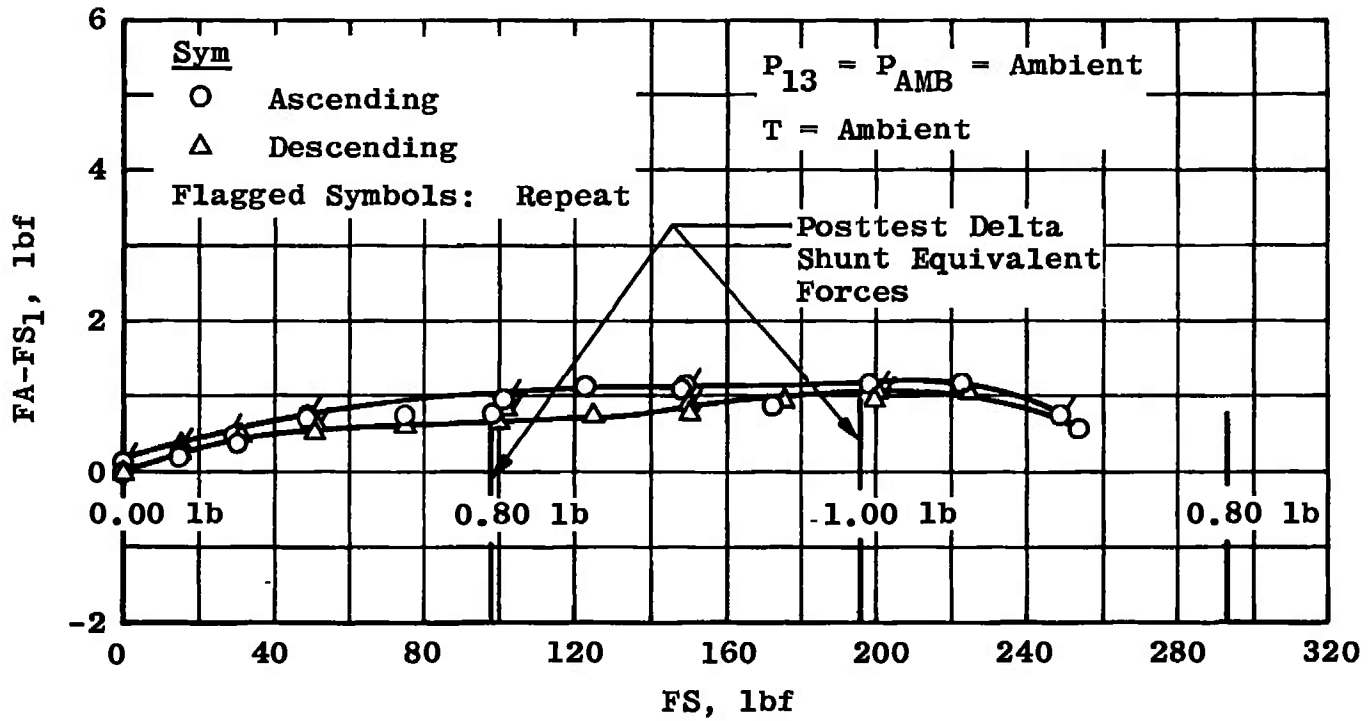$$T_4 = \,^\circ F$$

LOAD CELL PRESSURE CORRECTION

The scale force variation with environmental pressure sensed by the load cell is presented in Fig. C-4. The test cell pressure correction, obtained from Fig. C-4, was:

$$\Delta FS_P = 2.255 - 0.15747 \, (P_{AMB})$$

a. Pretest

Figure C-1. System tare at ambient conditions.
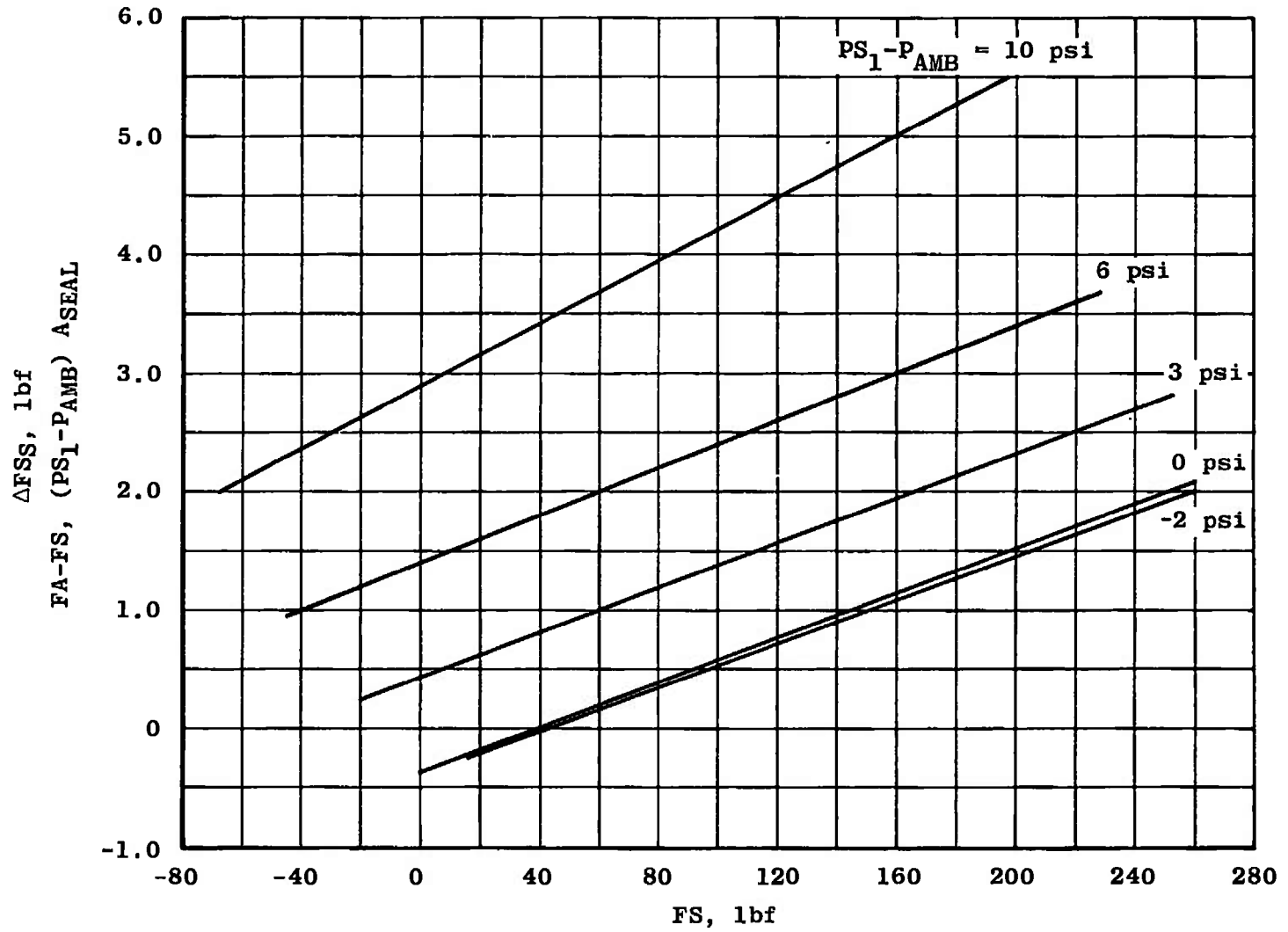
b. Posttest
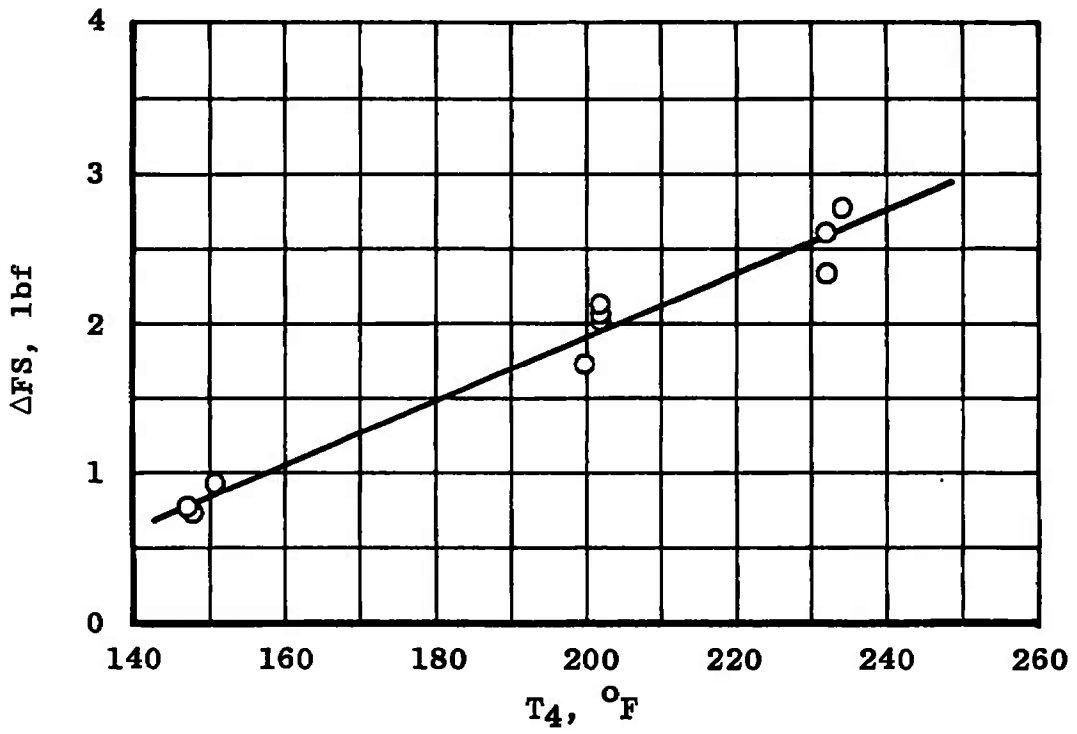Figure C-1. Concluded.

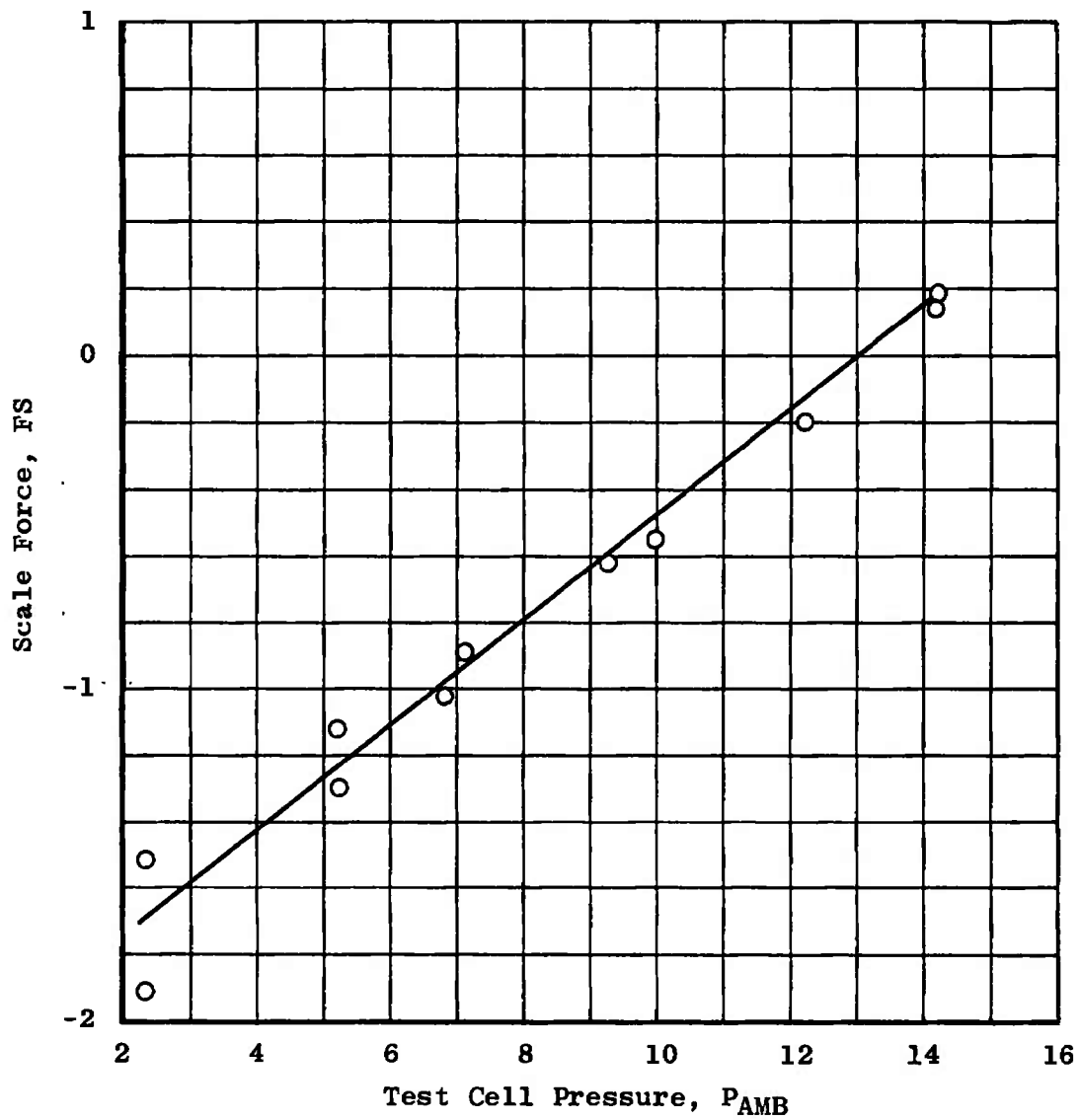Figure C-2. Inlet air seal tare.

Figure C-3. Temperature tare.

Figure C-4. Load cell pressure tare.

NOMENCLATURE

A	Area, in.^{2}
A_0, A_1, A_2	Coefficients for C_F equation
B_0, B_1, ..., B_6	Coefficients for C_{500}^* equation
C_d	Discharge coefficient
C_f	Flow coefficient
C_0, C_1, ..., C_5	Coefficients for C^* (P_{VI}) equation
C_p	Specific heat at constant pressure
C_t	Coefficient for effects of thermal growth
C^*	Critical flow factor
C_I^*	C^* for ideal gas
C_{500}^*	C^* at T = 500°R
C_{700}^*	C^* at T = 700°R
C_T^*	C^* for 500 ≤ T ≤ 700°R
D	Diameter, in.
D_0, D_1, D_2, D_3	Coefficients for F(T) equation
FG	Gross thrust, lbf
FS	Scale force, lbf
f(T)	Correction factor to C^* to account for total temperature
G	Acceleration of gravity, 32.174 ft-lbm/sec^2 lbf
M	Mach number
N	Rotor speed, rpm
P	Total pressure, psia

PS	Static pressure, psia
P^*	Venturi throat static pressure, psia
R	Gas constant, ft-lbm/lbf °R
Rn	Reynolds number
T	Total temperature, °F or °R
T_{ref}	Reference temperature for C_t (540°R)
TS	Static temperature, °F or °R
T^*	Venturi throat static temperature, °R
W, WA	Airflow rate, lbm/sec
W_{c_4}	Bearing cooling airflow rate, lbm/sec
a	Thermal expansion coefficient, °R^{-1} = 1.3 x 10^{-5} for alumium (compressor venturi) = 6.4 x 10^{-6} for mild steel (turbine drive and bleed venturi)
$\Delta C^*(P_{VI})$	$C^*_{500} - C^*_{700}$
γ	Ratio of specific heats
δ_2	Ratio of compressor inlet total pressure (P_2) to standard sea-level pressure (14.696 psia)
θ_2	Ratio of compressor inlet total temperature (T_2) to standard sea-level temperature (518.67°R)

SUBSCRIPTS

0 through 9	Instrumentation stations
AMB	Ambient
BM	Turbine bleed venturi
DM	Turbine drive venturi
I	Isentropic

IN	Compressor inlet
P	Calculation based on pressure
R	Corrected to standard sea-level conditions
S	Inlet air seal
T	Temperature
TTO	Thrust trim orifice
V	Velocity, ft/sec
VI	Turbine drive venturi inlet
VT	Turbine drive venturi throat
W	Calculation based on continuity